

Multi-Sensor Sheets Based on Large-Area Electronics for Advanced Structural Health Monitoring of Civil Infrastructure

Final Report
September 2014

Branko Glisic
Assistant Professor
Princeton University
Princeton NJ 08544

Thomas Schumacher
Assistant Professor
University of Delaware
Newark DE 19716

Raimondo Betti
Professor
Columbia University
New York NY 10027

External Project Manager
Nagnath Kasbekar, P.E.
Director, Bridge Engineering & Infrastructure Management
New Jersey Department of Transportation

In cooperation with
Rutgers, The State University of New Jersey
And
State of New Jersey
Department of Transportation
And
U.S. Department of Transportation
Federal Highway Administration

Disclaimer Statement

The contents of this report reflect the views of the authors, who are responsible for the facts and the accuracy of the information presented herein. This document is disseminated under the sponsorship of the Department of Transportation, University Transportation Centers Program, in the interest of information exchange. The U.S. Government assumes no liability for the contents or use thereof.

TECHNICAL REPORT STANDARD TITLE PAGE

1. Report No. CAIT-UTC-025	2. Government Accession No.	3. Recipient's Catalog No.	
4. Title and Subtitle Multi-Sensor Sheets Based on Large-Area Electronics for Advanced Structural Health Monitoring of Civil Infrastructure		5. Report Date September 2014	
		6. Performing Organization Code CAIT/Princeton	
7. Author(s) Branko Glisic, Thomas Schumacher, Raimondo Betti		8. Performing Organization Report No. CAIT-UTC-025	
9. Performing Organization, Name and Address Princeton University Princeton, NJ 08544		10. Work Unit No.	
		11. Contract or Grant No. DTRT12-G-UTC16	
12. Sponsoring Agency Name and Address Center for Advanced Infrastructure and Transportation Rutgers, The State University of New Jersey 100 Brett Road Piscataway, NJ 08854		13. Type of Report and Period Covered Final Report 1/01/13 - 9/30/2014	
		14. Sponsoring Agency Code	
15. Supplementary Notes U.S Department of Transportation/Research and Innovative Technology Administration 1200 New Jersey Avenue, SE Washington, DC 20590-0001			
16. Abstract Structural Health Monitoring has a great potential to provide valuable information about the actual structural condition and can help optimize the management activities. However, few effective and robust monitoring technology exist which hinders a nationwide use of SHM in on-site application for structural condition evaluations. The objective of this research was to develop and evaluate a prototype of a novel multi-sensor sheet that is inexpensive, can be equipped with a variety of different sensors, easy to fabricate and deploy, and which provides densely spaced quantitative measurements from large areas of a structure. This sheet is based on technology called large-area electronics and consists of dense arrays of sensors supporting several different electronic components (interconnects, circuits, batteries, etc.) that are patterned or laminated on a polyimide substrate. The sensors that can be incorporated in this sheet are, for example, strain gauges, temperature and humidity sensors, and piezoelectric transducers. At this stage, the development focused on strain sensors and piezoelectric transducers to address the challenges presented above. The design principles for sensing sheet were created. Prototypes were manufactured and successfully tested in laboratory under fatigue crack condition. Different configurations of sensors were tested to assess their performances. Data analysis algorithms were elaborated. The project description and outcomes are presented in detail in the report.			
17. Key Words Large area electronics, Structural health monitoring, Crack detection, Dense array of sensors, Strain monitoring, Acoustic emission		18. Distributional Statement	
19. Security Classification Unclassified	20. Security Classification (of this page) Unclassified	21. No. of Pages 37	22. Price

Acknowledgments

The large-scale tests on steel plates equipped with sensing sheets were carried out at the Carleton Laboratory in Columbia University. Steel specimens and associated accessories were provided by the University of Delaware. Sensing sheets were provided by Princeton University.

The authors would like to thank Y. Yao, S-T. E. Tung, D. Smith, Prof. N. Verma, Y. Hu, L. Huang, N. Lin, W. Rieutort-Louis, J. Sanz-Robinson, T. Liu, Prof. J. C. Sturm, and Prof. S. Wagner, all from Princeton University, for their precious advice and help in the project. Furthermore, thanks go to L. Mhamdi, A. Tabrizi, N. Ramanna, and G. Wenczel from the University of Delaware for assisting with testing and data analysis. Final thanks go to L. Li and E. Sporer from Columbia University for precious help in realization of fatigue test.

Table of Contents

	Page
DESCRIPTION OF THE PROBLEM	1
APPROACH	2
METHODOLOGY	2
FINDINGS	3
CONCLUSIONS	23
RECOMMENDATIONS	25

List of Figures

Figure 1. Left: top view of the experiment setup. Right: positioning of the sensor 90° to the crack (source: Tung et al. 2014, see journal papers in Conclusions).	4
Figure 2. Crack opening vs. strain for Type 1 tests up to 5000 $\mu\epsilon$. Mean \pm one standard deviation and lognormal distribution for the calibration coefficient shown (source: Tung et al. 2014, see journal papers in Conclusions).	5
Figure 3. Experimental setup for cracked tests.	6
Figure 4. Left: Strain and concrete temperature against time (crack width = 0 μm). Right: Strain against temperature for cracked tests (crack width = 0 μm).	6
Figure 5. Left: Analytical model of the probabilistic problem of crack detection. Middle: shaded areas are detectable angles. Right: Results of analytical solution (black line) and two MC simulations (blue and red curves) for $P(D L)$ in a given surface area.	8
Figure 6. Left: Disperse arrangement of sensors (design “SS1”). Right: Dense arrangement of sensors (design “SS2”). In tests, the crack propagates from “A” towards “I”.	8
Figure 7. Left: Design 1 with rectangular array of Piezoelectric discs (design “AE1”). Right: Design 2 with circular array of Piezoelectric discs (design “AE2”).	9
Figure 8. Photo of the steel test specimen. The area within the dotted line represents the location of the prototype multi-sensing sheet. Dimensions in inches.	10
Figure 9. Left: Example of PCB design of sensing sheet interconnect (for strain sensing sheet prototype shown in Figure 2 left). Right: Interconnect manufactured based on the PCB design.	10
Figure 10. Left: Installation of individual sensors onto the sensing sheet; Middle and right: complete assembly of sensing sheets as per design shown in Figure 6.	11
Figure 11. Left: application of adhesive. Right: spreading the adhesive over the intended area of installation.	11
Figure 12. Four steel plate equipped with sensing sheets.	12

	Page
Figure 13. Left: crack detection on a real concrete structure using long-gauge fiber optic sensors and threshold-based algorithm; Right: schematic representation of the 2D LAE sensing sheet, its application, and determination of damage extent.	14
Figure 14. Schematic showing steps in phased array processing, i.e. beam forming.	14
Figure 15. Parameters for beam forming using circular array.	15
Figure 16. Results from synthetically simulated data for two assumed angles: (a) 169.2 Degrees and (b) 45.0 Degrees (correct angle).	15
Figure 17. Total response for angles from 0 to 180 Degrees: (a) Cartesian plot, (b) polar plot.	16
Figure 19. Test setup to evaluate piezo-electric discs and circular arrays.	16
Figure 19. Example result from actual AE: (a) Individual signals, (b) total response for the angle corresponding the maximum response, results in (c) Cartesian coordinates, (d) polar coordinates.	17
Figure 20. Left: fatigue test setup and test fixture; Middle: installation of specimen; Right: specimen insulated with duct tape, placed into the testing frame, secured with the fixtures, and connected with cables (to the reading unit).	18
Figure 21. Left: Strain signal reading unit of Princeton University; Middle: Acoustic emission signal reading unit of University of Delaware; Right: MTS displacement and load control system of Columbia University.	18
Figure 22. Initial crack occurring in Specimen No. 1 (left) and No. 2 (right).	20
Figure 23. Typical failure modes of the sensing sheet under excessive crack opening; Left: delamination, Sample No.; 3; Right: tearing, Specimen No. 4.	20
Figure 24. Typical sensor readings, Specimen No. 4	21
Figure 25. Propagation of crack from location “D” to location “G”.	22

List of Tables

Table 1. Design specifications of specimens equipped with sensing sheets.	12
Table 2. Piezo-electric discs selected for this study.	16

DESCRIPTION OF THE PROBLEM

Many bridges in the country have reached their intended service life limit [1, 2]. Some of them do not pass current load-ratings or show deterioration such as corrosion and cracking. Money for replacement and repair of bridges, however, is scarce. In order to keep these critical infrastructure components in operation, inspection, maintenance, and monitoring play a vital role. Structural Health Monitoring (SHM) has great potential to provide valuable information about the actual structural condition and can aid in early detection and evaluation of damage and deterioration that are invisible to the human eye. However, few effective and robust monitoring and data analysis techniques exist which hinders a nationwide use of SHM in structural condition evaluations.

One pressing problem is fatigue cracking in fracture critical bridge members, which can have disastrous consequences to the infrastructure and public safety [3-5]. Because detection of fatigue cracks can be difficult, it is essential that a sensing technology is utilized that is able to measure strains at a large number of points with high accuracy. One challenge by deploying a traditional array of strain gages or strain rosettes is the complexity in the wiring. Also, for reinforced or prestressed concrete structures, damage that may lead to catastrophic failure is typically associated with internal processes such as wire fracture that may not necessarily be detectable on the surface [6, 7]. Acoustic Emission (AE) monitoring techniques represent a possible solution to this problem [8, 9]. Often, however, it is not feasible to install a dense network of AE sensors due to the prohibitive costs associated with such a system.

Current available technologies give bridge managers access to sparsely spaced sensors. These, unfortunately, do not allow reliable early detection of anomalies such as strain concentrations or cracks at locations of even modest distances away from the sensor. To infer localized anomalies, such forms of indirect sensing rely on complex algorithms whose reliability is challenged by practical noise sources (i.e., temperature, precipitation, and normal loading variability). Thus, a need exists for a cost-effective sensing approach that is able to incorporate a variety of sensors applied in form of very dense arrays to maximize the chances for capturing damage externally as well as internally at an early stage. The measurements should support the bridge owners for informed decision making. Our research addresses the need for direct sensing, where anomalies are sensed at close proximity via a dense array of sensors.

The objective of this research was to develop and evaluate a prototype of a novel multi-sensor sheet that is inexpensive, can be equipped with a variety of different sensors, easy to fabricate and deploy, and which provides densely spaced quantitative measurements from large areas of a structure. This sheet is based on technology called large-area electronics and consists of dense arrays of sensors supporting a variety of electronic components (interconnects, circuits, batteries, etc.) that are patterned or laminated on a polyimide substrate [10]. The sensors that can be incorporated in this sheet are, for example, strain gages, temperature and humidity sensors, and piezoelectric transducers. At this stage, the development will focus on strain sensors and piezoelectric transducers to address the challenges presented in the introductory section of this proposal.

APPROACH

Materials fail at a point when the stress at that point exceeds the ultimate limit state, i.e. the strength at that point. Strain is a parameter directly correlated to stress, and so any change in the stress field is reflected through a change in the strain field. There is no effective means to directly monitor stress under real, on-site conditions; consequently, strain (static and/or dynamic) has emerged as an important parameter in SHM [11-13]. The first signs of damage to a structure often have local character and occur in the form of strain-field anomalies. Typical examples are cracks and bowing in steel (which are early indicators of fatigue and loss of local stability), as well as non-structural cracks in concrete (which are early indicators of damage caused by frost, alkali-reaction, or corrosion in reinforcing bars and prestressing cables). To address these problems, a variety of options have become available for strain anomaly sensing, including methods that combine various sensing modalities. In our research we will focus on integrating strain sensors based on the electrical resistivity principle and Acoustic Emission (AE) transducers that operate based on the piezoelectric effect. In this manner, occurring surface and sub-surface damage can be detected simultaneously. Both general sensing principles have proven reliable over the years of use and that is the reason for their selection in this project.

The sensing technology that will be studied in this work consists of the following: (1) 2-D distributed arrays of (a) resistive strain gages and (b) piezoelectric transducers on a polyimide substrate combined with functional large-area electronics; (2) embedded integrated circuits (IC) interfaced via non-contact links for sensor read-out, data aggregation, and data analysis; and (3) integrated solar-energy harvesters and power converters on the large-area-electronics sheet for full-system self-powering. The part (1) was explored in details, while parts (2) and (3) were studied at the proof-of-concept level in collaboration with researchers at the Department of Electrical Engineering of Princeton University (at no cost).

METHODOLOGY

The methodology applied in the project is briefly presented below, followed by a detailed description at the end of the section.

(1) Sensing sheet specifications

Task 1.1: Detailed literature review {1, 2}

Task 1.2: Establishment of sensing sheet specifications through theoretical considerations and reduced-scale laboratory testing of sensing sheet components (distance and orientation of sensors, sensitivity to damage) {1, 2}

(2) Creation of sensing sheet prototype

Task 2.1: Evaluation of manufacturing techniques (lamination vs. patterning) {1}

Task 2.2: Manufacturing two sensing sheet prototypes {1, 2}

(3) Data analysis

Task 3.1: Exploration and development of data analysis algorithms for strain sensors {1}

Task 3.2: Exploration and development of data analysis algorithms for Acoustic Emission transducers {2}

Task 3.3: Expert review on data analysis algorithms and their integration {3}

(4) Laboratory experiments

Task 4.1: Test 1: detection of steel fatigue cracks in large-size specimens using a sensing sheet prototype {3}

{1} performed at Princeton University

{2} performed at the University of Delaware

{3} performed at Columbia University

The first task investigated theoretically and experimentally how the density and arrangement (orientation, positioning, etc.) of strain sensors and piezoelectric transducers affects the sensitivity of localized damage sensing; this served to establish specifications for the prototype sensing sheet. The second task pursued the creation of the requisite sensing sheet as an experimental prototype. The third task investigated methods for analyzing the resulting sensor data for damage detection in order to evaluate the viability of utilizing simple computational approaches using the collected data. Finally, the fourth task evaluated the sensitivity and potential for enhanced detection afforded by direct sensing by way of the prototype sheet; a quantitative comparison under laboratory conditions was made against fiber-optic sensors available through the PI Glisic and commercial AE sensing equipment provided by the Co-PI Schumacher. In this final task, four large-scale experiments were conducted in the Co-PI Betti Structural Laboratory. Tests involved a steel specimens with a fatigue crack that were tested under cyclic fatigue loads to evaluate the sheets capability to detect fatigue crack initiation and growth. The sensing sheets were be manufactured by lamination at Princeton University and University of Delaware premises. Tests on individual sensor components were performed at Princeton University (strain sensors) and the University of Delaware (piezoelectric transducers). System tests (completed sheet) on large-scale specimens were performed at Columbia University. The plan is to apply for funding for a phase II research project to perform on-site tests at the NJ23/US202 Overpass in Wayne, NJ (part of FHWA's LTBPP).

FINDINGS

Sensing sheet specifications

Feasibility of incorporating strain sensors and piezoelectric transducers in the sensing sheets based on large area electronics technology was studied and proved true. Literature review on different types of structural cracks and crack detection and characterization techniques was also performed and a review paper published (see Conclusions). Series of tests and computational simulations were performed and they are presented as follows.

Sensitivity of thin resistive strain sensor to crack opening

The main focus of this test was to examine the relationship between crack opening and measured strain for thin resistive full-bridge strain sensors. Full-bridge sensors were used because of their capability for differential sensing. This significantly improves robustness against noisy signals from external sources and helps avoid large sinusoidal baseline signals that would affect the AC readout scheme applied to the sensing sheet. Since the cost of manufacturing prototypical sensing sheets is very high, less expensive commercial strain gauges were used in this study. This simplification is justified because similar sensors will be patterned on the aforementioned sensing sheets in the future. This research mainly focused on cracks oriented

perpendicular (90°) to the strain gauge, but other orientations were tested as well. In order to achieve repeatable results, all experiments were conducted in a controlled laboratory environment with the same preparation and testing procedure. Each experiment involved mounting a small artificially cracked concrete slab to a micrometer stage and bonding a commercially available full-bridge sensor (gauge length = 14.8 mm) over the crack. High-strength epoxy was used in both the concrete-stage interface and the concrete-sensor interface. The micrometric screw attached to the stage controlled and adjusted the crack width, and strain readings were taken by appropriate reading unit. Experiments were stopped either when the strain sensor was broken or when the measuring range of the reading unit was overpassed. A schematic view to the test set-up is shown in Figure 1.



Figure 1. Left: top view of the experiment setup. Right: positioning of the sensor 90° to the crack (source: Tung et al. 2014, see journal papers in Conclusions).

Results of ten tests are illustrated in Figure 2. For each test, strain change of the same order of magnitude is found for every crack opening increment, which indicates linear relationship. The strain change (tension) measured by the sensor was very high for each crack increment, and the values ranged between several hundred to several thousands of microstrain, which is an order of magnitude higher than usual strain variations in structures due to live loads. The high sensitivity of the strain sensors to crack openings was thus confirmed by this test, and crack opening was successfully detected by the direct strain measurement. While all ten experiments produced nearly linear results, the large dispersion of gradients suggests that there are other factors besides crack growth that affect the strain response. The variation is probably due to the magnitudes of initial crack widths; stress concentrations at the edges of the crack; and the deterioration of the concrete from the epoxy. Also, it was difficult to keep all ten procedures completely identical even though the sample preparation was standardized. Thus, while the crack detection and localization using sensing sheets with integrated sensors is expected to be reliable, an estimation of the crack size would require additional statistical data analysis by introducing probability density function, as shown in Figure 2.

The results of statistical analysis have several important implications regarding the capability of full-bridge strain sensors for crack quantification. Figure 2 shows that the calibration coefficients are likely to be lognormally distributed, which implies that we cannot deterministically evaluate the width of the crack; however, we can predict the width of a crack using a probabilistic approach. For example, if the apparent strain (sensor reading) changes for $3,000 \mu\epsilon$, we can conclude that a crack occurred. Its expected crack opening is $121 \mu\text{m}$, but the most likely value of the crack opening is $95 \mu\text{m}$. The lognormal distribution also implies that there is a 73% chance that the width is between 70 and $173 \mu\text{m}$ (\pm one standard deviation from

the mean) and a 96% chance that the width is between 18 and 224 μm (\pm two standard deviations from the mean). This probabilistic approach may seem vague or inconclusive; however, it should be observed at a sensing sheet scale: a crack occurring in the structure will certainly affect several sensors in the sensing sheet, and the probabilistic information about crack size obtained from multiple sensors can then be used to infer the size of the crack.

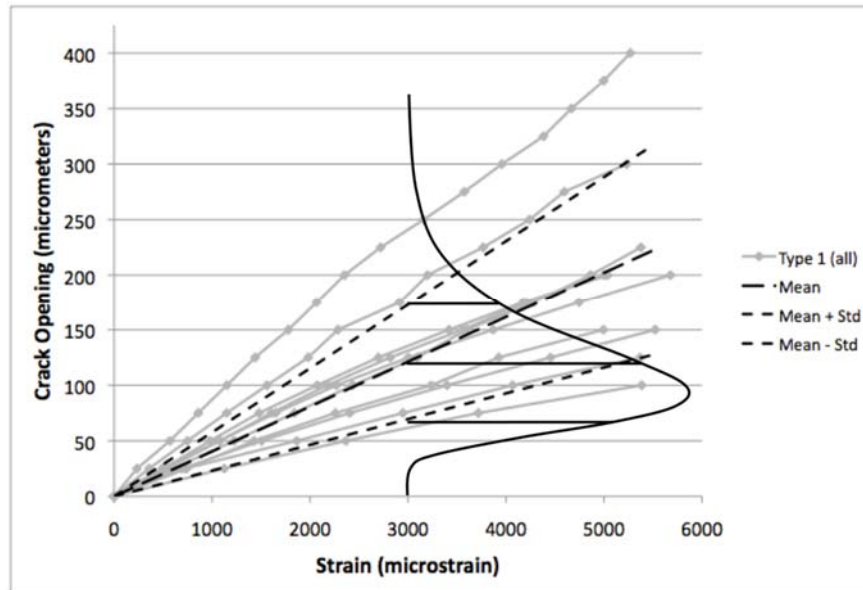


Figure 2. Crack opening vs. strain for Type 1 tests up to 5000 $\mu\epsilon$. Mean \pm one standard deviation and lognormal distribution for the calibration coefficient shown (source: Tung et al. 2014, see journal papers in Conclusions).

Response of Full-Bridge Strain Sensors to Thermal Variations

In on-site conditions the thermal influence to the individual sensor may represent the major issue in data analysis. Hence, the main focus of this activity was to investigate the response of individual full-bridge strain sensors when they are subjected to different temperatures. This study uses commercial strain sensors (Omega SGT-4/1000-FB13, gauge length = 7.4 mm) due to their low cost. Since similar sensors will be patterned on the sensing sheet, their replacement with commercially available strain sensors does not reduce the validity of the results. The response to temperature was tested in laboratory. In order to achieve repeatable results, all experiments were conducted in a controlled environment with the same preparation and testing procedure. In general, there are two different temperature experiments: “uncracked” tests and “cracked” tests. Uncracked tests involve bonding a single strain sensor to an uncracked concrete slab and exposing it to variable temperature conditions. Cracked tests involved mounting an artificially cracked concrete slab to a micrometer stage, see Figure 1. The micrometric screw attached to the stage controlled and adjusted the crack width. The set-up was then put in the oven and exposed to variable temperature conditions.

For all cracked tests, the sensor was attached to a reading unit (NI cDAQ-9178 Chassis with NI 9219 Modules) with crocodile clips. Additionally, two K-type thermocouples were used: one was insulated and attached to the concrete surface, while the other was not insulated and positioned in the air above the sensor. Each concrete slab was only used once, but the same

micrometer stage for all cracked experiments. The experimental setup is shown in Figure 3.

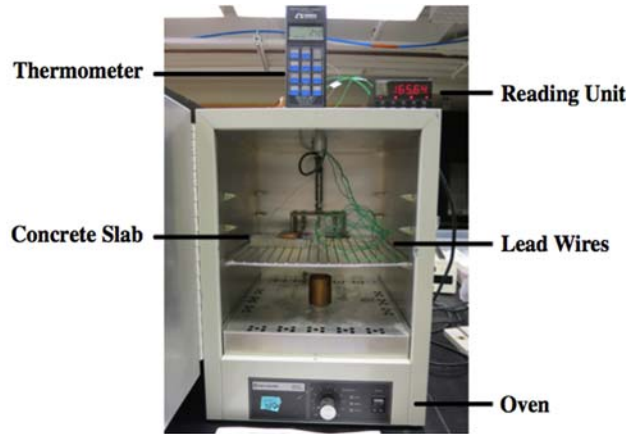


Figure 3. Experimental setup for cracked tests.

The uncracked test showed that thermal influence to the individual full-bridge sensor can be neglected (it is in order of $-1 \mu\epsilon/^\circ\text{C}$). This result was expected based on analytical modeling and it is very important as it shows that temperature variations are not likely to be confused with the damage. The results of the Cracked tests are shown in Figure 4. The left image of Figure 4 is a diagram of strain and concrete temperature against time for the duration of three heating cycles for crack width = $0 \mu\text{m}$. It shows that there is a positive relationship between measured strain and concrete temperature. As shown by Sample B and C (see the figure), the relationship between strain and temperature becomes consistent after the first full heating cycle. This is because the first cycle “sets” the interacting materials (sensor, glue, micrometer stage) in the system. The first heating cycle for Samples A, D, and E were heated straight to 58°C (setting #4) and cooled back down to 28°C (setting #2) and the results for the second and third heating cycles are very similar to Samples B and C. The right image of Figure 2 is a plot of strain against temperature for all cracked experiments with crack width = $0 \mu\text{m}$.

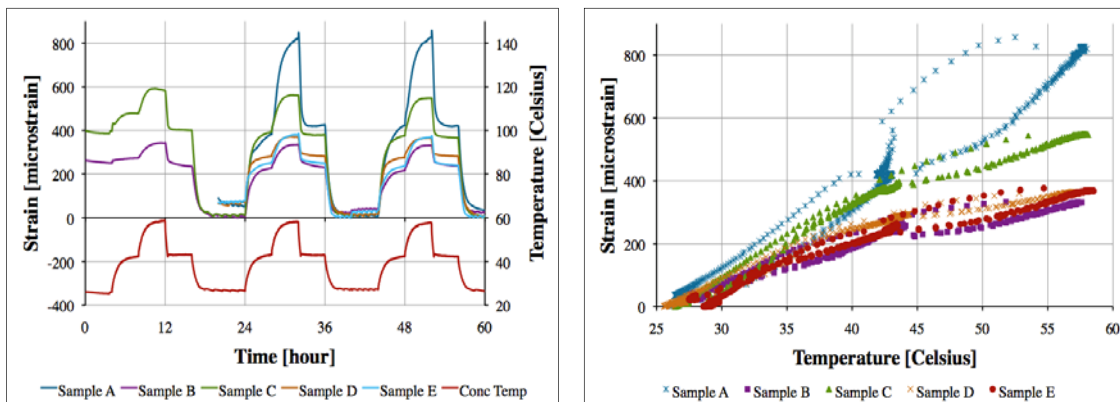


Figure 4. Left: Strain and concrete temperature against time (crack width = $0 \mu\text{m}$). Right: Strain against temperature for cracked tests (crack width = $0 \mu\text{m}$)

Cracked tests demonstrate that temperature change actually amplifies the strain reading at the location of the damage. While this has positive effect in terms of damage detection, it has negative effects in terms of damage quantification.

Design of the strain sensing sheet based on probabilistic approach

The sensing sheet contains very dense arrays of sensors, but although the sensors are densely spaced, there are some non-instrumented spaces between them and these spaces are not sensitive to minute damage. Probabilistic approaches in damage detection can help practical evaluation of the damage. One of the approaches is to design the sensor network based on probability that this particular network can detect a damage of certain size. This approach evaluates the probability of minute-crack detection of innovative sensing sheet based on LAE. First, analytical or numerical method is used to evaluate overall probability that damage of any size can occur in area covered by the sheet. Then, based on above probability the size and spacing of sensors can be determined so the sensing sheet can detect the damage with desired probability.

As an initial step, the goal of this research is to determine the probability of crack detection for a single sensor. A geometric probabilistic method was used to find the analytical solution, and two Matlab simulations based on Monte Carlo method were created to generate numerical solutions to the problem. The problem is approached geometrically by assuming any orientation and size of crack (Figure 5 Left), and “visualizing” each crack as the diameter of a circle (circle is defined by midpoint of the crack, and diameter is the length of the crack). As shown in the middle image of Figure 5, the shaded areas are “detectable angles”. For a given crack length L , if a crack is rotated and it is within a detectable angle, then the sensor will detect the crack. If the crack center (the black dot) is within the sensor then the crack will be detected since all angles are then detectable angles. On the other hand, if the crack center is too far from the sensor (circle does not intersect the sensor), it will have no detectable angles and its POD is zero. According to the total probability theory, the POD for a crack with length L is expressed as follows:

$$P(D|L) = \sum P(D|LA_i)P(A_i)$$

where $P(D|LA_i) = \frac{1}{A_i} \iint \frac{\theta_i}{\pi} dx dy$ and $P(A_i) = \frac{A_i}{A_{total}}$. If the crack lengths are uniformly distributed between L_1 and L_2 , the overall POD is $P(D) = \int_{L_1}^{L_2} P(D|L) P(L) dL$. As a result, the analytical solution is: $P(D|L) = \frac{2L(b+h)+\pi bh}{BH\pi}$. Where b and h are the sensor dimensions, and B and H are the surface area dimensions.

Results of both the analytical and numerical solutions are compared, and these results can be further applied to study the probability of damage detection with more sensors, i.e. the whole sensing sheet. The probability of detection (POD) is essentially a metric used to quantify the reliability of inspection systems, so the effectiveness of different SHM techniques is usually characterized by a POD curve that relates the size of damage to the probability of correct detection. Figure 5 below shows the analytical model of this probabilistic problem and typical results of both analytical solution and MC simulations, which have a great consistency. Thus, developed MC simulations can be used for assessment of POD.

The POD was tested for different arrangements of sensors and as the result of modeling the sensing sheet configurations shown in Figure 6 are selected. Figure 6 left shows more disperse arrangement of sensors while Figure 6 right shows dense arrangement, and the challenges and advantages of these two configurations were studied in the project.

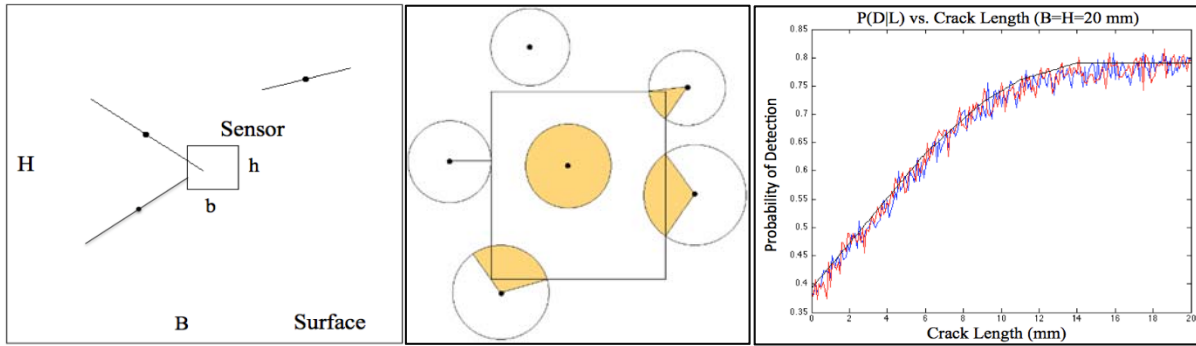


Figure 5. Left: Analytical model of the probabilistic problem of crack detection. Middle: shaded areas are detectable angles. Right: Results of analytical solution (black line) and two MC simulations (blue and red curves) for $P(D|L)$ in a given surface area.

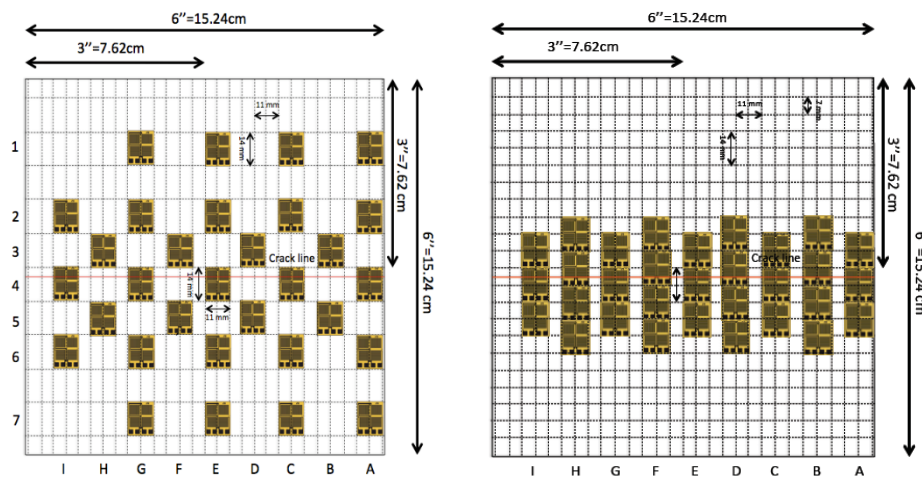


Figure 6. Left: Disperse arrangement of sensors (design “SS1”). Right: Dense arrangement of sensors (design “SS2”). In tests, the crack propagates from “A” towards “I”.

Design of acoustic emission (AE) sensing sheet

Complimentary to the strain sensors, the goal of this research is to evaluate the implementation of an acoustic emission (AE) methodology into multi-sensing sheets. There are two main sensor arrays that we propose to evaluate as illustrated in Figure 7. Characteristics of the piezoelectric discs selected for these arrays are presented later in Table 2.

Both of these arrays have their strengths and limitations: Traditional arrays (Figure 7 left) are used to locate sources in two dimensions originating from within the sensor array boundaries and theoretically allow for quantitative AE analyses such as moment tensor inversion (MTI) if at least four to six high-quality (i.e. low noise) signals are available. The information used to locate and characterize a source is based on the first wave arrival at each sensor, i.e. the p-wave arrival. Typically, iterative methods based on the one originally proposed by Geiger (1910) are used. Before the source location coordinates can be estimated, p-wave arrival times need to be picked accurately. This type of array is very sensitive to uncertainties if a source lies outside the array boundaries, which results in large errors. Phased arrays (Figure 7 right) are used to point to the direction of source origins that lie away from the array boundaries and work even with low signal quality. This type of array only works for sources that are far away from the source so that

the assumption of a parallel wave field is acceptable (see Figure 8). A quantitative analysis is not possible. In this case, no arrival time picking is necessary. A more detailed description is presented in the analysis section of this report.

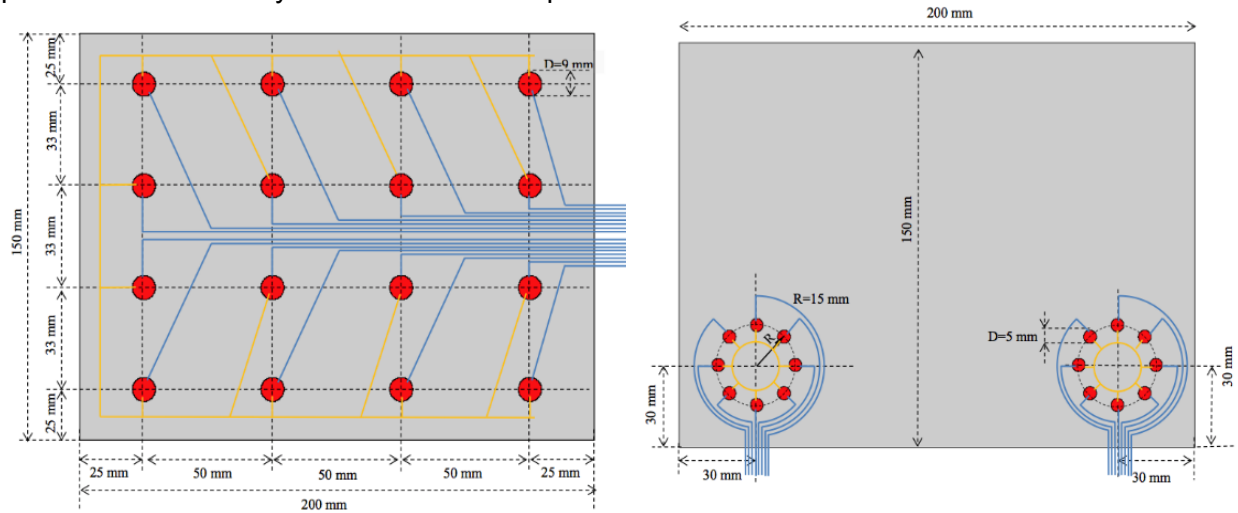




Figure 7. Left: Design 1 with traditional array of Piezoelectric discs (design “AE1”). Right: Design 2 with circular phased array of Piezoelectric discs (design “AE2”).

In order to select appropriate piezoelectric discs for the AE arrays, the following tests were performed. Each disc was mounted on a steel plate and subjected to a Morlet-type wave generated by a piezo-electric actuator and its response evaluated. Two discs that showed reasonably consistent response over a frequency range of approximately 400 to 1000 kHz were selected and are listed in Table 1.

Table 1. Piezoelectric discs selected for AE arrays.

PZT	Diameter (mm)	Thickness (mm)	Resonant Frequency	Vibration Mode	Array
	9	0.4	5 MHz	Thickness	AE1 (rectangular)
	5	0.4	450 KHz	Thickness	AE2 (circular)

For both of the array types, algorithms to locate AE sources were implemented and tested using artificial sources prior to laboratory testing, as shown in the section of this report that addresses the data analysis.

Creation of sensing sheet prototype

Evaluation of manufacturing techniques (lamination vs. patterning)

In order to decrease the cost of manufacturing of the sensing sheet prototypes, it was decided to proceed with the hybrid solution, i.e., to pattern the interconnect of the sensing sheet and then to laminate commercially available strain and AE sensors onto the interconnect. The

lamination was initially intended to be performed using double-sticking tape conductive in perpendicular direction; however, it was later shown that the use of ordinary tape is simpler and more practical solution, as the adhesive used to attach the sheet to monitored structure can also ensure the contact between the sensors and the interconnect.

Manufacturing of sensing sheet prototypes

The interconnect allows multiple sensors arranged on the sensing sheet to be connected with the reading units. It consists of system of conductors patterned over Polyimide (Kapton) substrate. Design and manufacturing of the interconnect are important steps toward creation of the sensing sheet. The design of the interconnect strongly depends on the sensitivity and size of individual sensors and the data analysis approaches (see the next subsection). The size of the sensing sheet prototypes is determined based on the dimensions of large-scale steel test specimens, shown in Figure 8. The steel specimen in Figure 1 represents a compact specimen according to ASTM E647-08.

In total four arrangements of individual sensors for the sensing sheet were considered, two for strain sensors and two for AE sensors, as shown in Figures 6 and 7. The designs of interconnect for strain sensing sheets are shown in Figure 9. The strain sensing sheets are 6 x 6 inch, and accommodate for 31 individual strain sensors in both cases.

An example of printed circuit board (PCB) drawing (based on the design shown in Figure 6 left), necessary for the purpose of manufacturing is shown in Figure 9 left. The PCB design schematically depicts the electric circuit and connections of the sensing sheet. The corresponding example of the sensing sheet interconnect as manufactured is presented in Figure 9 right.

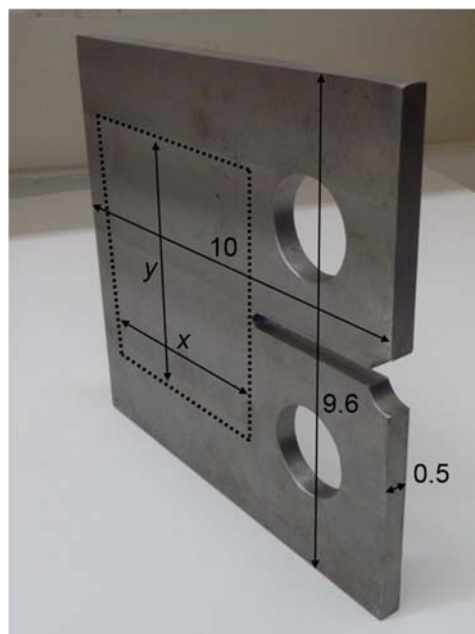


Figure 8. Photo of the steel test specimen according to ASTM E647-08. The area within the dotted line represents the location of the prototype multi-sensing sheet. Dimensions in inches.

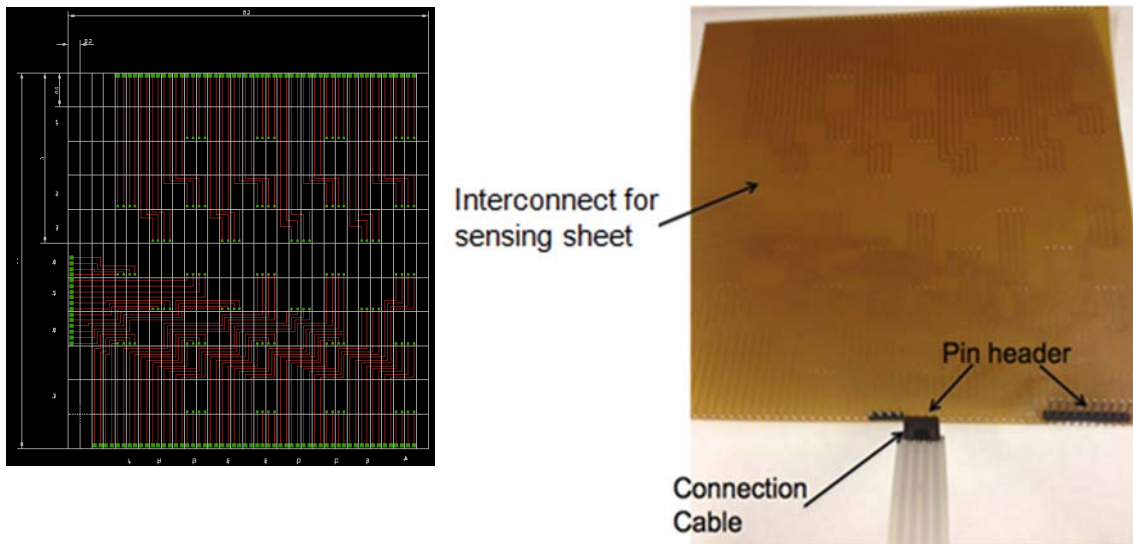


Figure 9. Left: Example of PCB design of sensing sheet interconnect (for strain sensing sheet prototype shown in Figure 2 left). Right: Interconnect manufactured based on the PCB design.

The interconnect contained two layers: the top layer, filled with metal conducting wires, and the bottom layer, filled with hollow metal pads that were connected to the wires on top layer. In order to protect the metal wires from cracks and avoid short circuit, individual strain gauges were laminated on the bottom side of the sensing sheet, with a small piece of ordinary tape to maintain their relative positions before installation onto the steel specimen (see Figure 10, left). The four connecting wires of the strain gauge were passed through the metal holes and contacted with the conducting wires on top layer. Photos of complete assembly of individual sensors onto the two different interconnects are shown in Figures 10 middle and right.

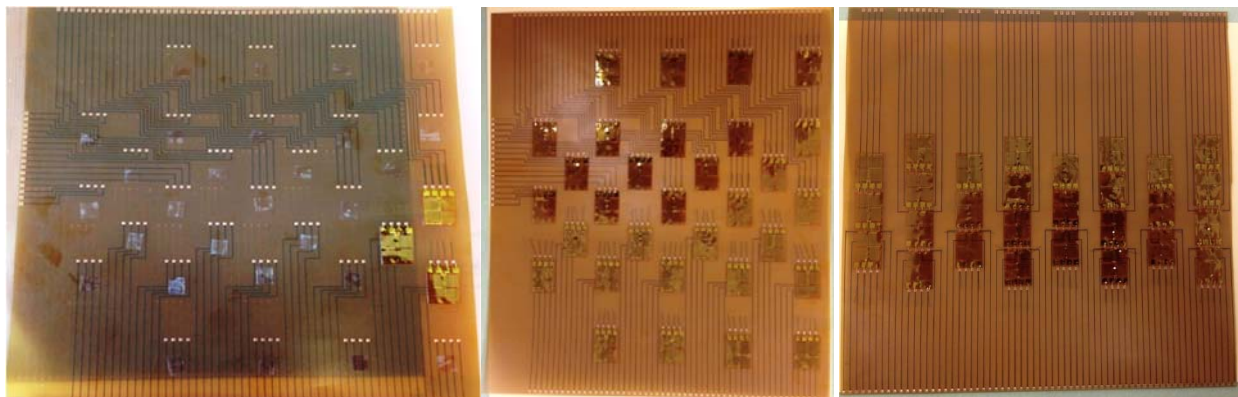


Figure 10. Left: Installation of individual strain sensors onto the sensing sheet; Middle and right: complete assembly of sensing sheets as per design shown in Figure 6.

After all the individual strain sensors were laminated onto the interconnect, they were glued to the test specimens. Figure 11 depicts the process of application of adhesive. The adhesive used is Araldite 2012.

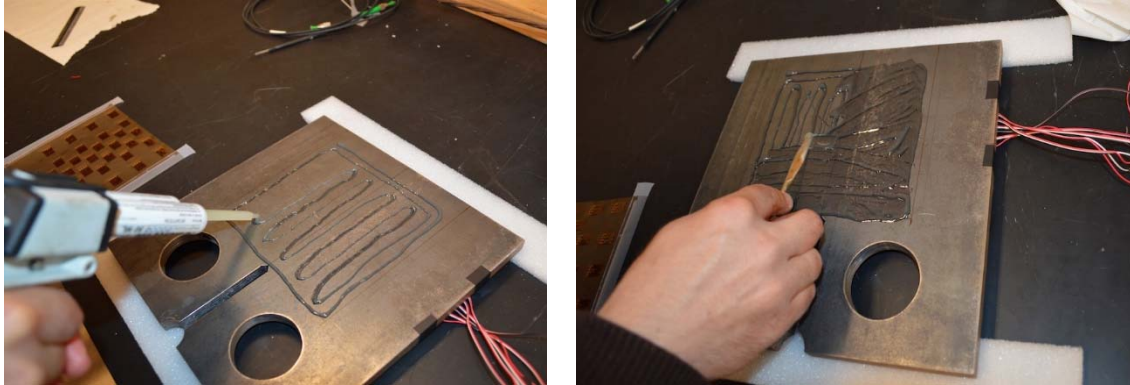


Figure 11. Left: application of adhesive. Right: spreading the adhesive over the intended area of installation.

Soon after the adhesive was applied, the sensing sheet was glued to the steel plate. It was important to ensure that there was no air bubble between the sensing sheet and the plate, thus, to guide the air bubbles out, a pressure was applied by hands and cloth over the glued sensing sheet before the adhesive hardened.

The AE sensing sheets were fabricated accordingly. First, the piezoelectric discs were glued to the specimen surface at the correct location using standard superglue. The PCBs were then adhered to the steel plate using the same principles as for the strain sensing sheets. Finally, solder tabs were placed to connect the piezoelectric discs with the interconnect.

A total of four steel plate specimens were equipped with sensing sheets as shown in Table 2. Each plate hosted a strain sensing sheet on one side of the plate, and an AE sensing sheet on the other side of the plate. Since there were two designs for strain sensing sheets (Figure 6) and two for AE sensing sheets (Figure 7), each plate was equipped with a different combination of the two technologies. The four sensing sheet designs are presented in Figure 12.

Table 2. Design specifications of specimens equipped with sensing sheets.

Specimen No.	Design
1	SS2-AE2
2	SS1-AE2
3	SS2-AE1
4	SS1-AE1

All the individual strain sensors belonging to all four sheets were tested immediately after the installation and all of them worked properly. The same was done for the AE sensing sheets where the response of all individual piezoelectric discs was verified using pencil lead breaks. However, it was noticed later, during the tests, that some sensors would lost the contact with the interconnect due to vibration, which indicated that lamination process should be improved by soldering the sensor leads to the interconnect pads. Thus, some sensors did not work during the tests as shown later in the text in the section describing the test results.

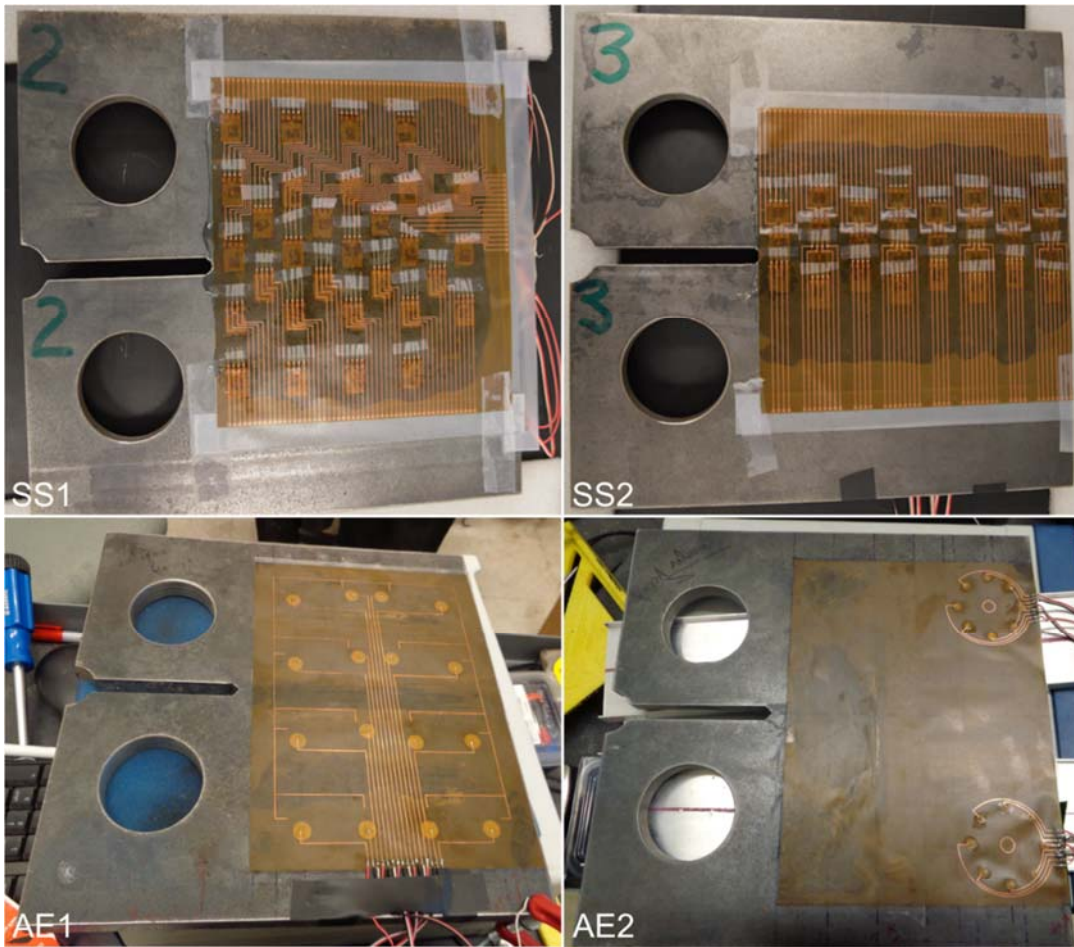


Figure 12. Four sensing sheet designs after gluing.

Data analysis

Exploration and development of data analysis algorithms for strain sensors

The data analysis for strain sensors is based on (1) evaluation of damage size based on probabilistic approach (see Section “Sensing sheet specifications” and Figure 2), (2) evaluation of Probability of Detection (see Section “Sensing sheet specifications” and Figure 5), and (3) threshold settings. The former two approaches are presented earlier in the report, while the latter is presented here in more details.

Pathological strain-field anomalies (e.g. cracks) will cause large changes in strain sensor readings (e.g. more than order of magnitude greater than usual strain variations, see Figure 13 left) and they will involve several sensors (e.g. as in Figure 13 right). These changes in practice can occur in short terms (typically cracks in steel and concrete develop within few minutes to few hours) or in long terms (typically yield or strength levels are reached gradually over several months to several years due to slow deterioration phenomena). Based on PI Glisic’s previous research, damage detection algorithms will be based on thresholds, applied both “in space” (i.e., over the sensed area) and “in time” (i.e., against previously collected measurements). The criteria are summarized as follows:

1. At least m neighboring sensors experience “unusually-high strain reading” at time t , with respect to reference time t_0 , where t_0 can be set to initial reference value (e.g., beginning of monitoring, or some later fixed time), or it can be variable based on the length of time interval to be examined (e.g., t_0 can be set few minutes / hours before the actual time t , where time interval $t-t_0$ represents the moving “window” of recent measurements); the “unusually-high strain reading” is defined either by a deterministic threshold (e.g., d microstrain, as indicated in the data presented in Figure 13 left) or a statistical threshold (e.g., (i) s multiples of the standard deviation σ observed over a window of recent measurements, or (ii) the standard deviation of current measurements over a local region of sensors).

Another simple statistical method that will be examined within the statistical analysis is modified “Z-score” method. This derives statistical thresholds based on the root-squared deviation from the median (i.e., rather than the mean), which has shown superior performance in some cases due to its robustness against outliers. The algorithms presented in this point can be applied for damage detection in both short and long terms, depending on the choice of reference time t_0 and the observed window of measurement.

2. The strain from at least k neighboring sensors reaches $p\%$ of the ultimate strain limit of the monitored material (e.g. 85%). This detects slow strain changes that are undetectable by criteria such as those presented in Point 1 above. Such degradations are nonetheless important as they can gradually reach critical levels.

3. Assuming that the damage is detected, the location and spatial extent of the damage can then simply be determined by identification of locations (coordinates) of sensors activated by the damage. Example in Figure 13 right illustrates this concept: the damage is represented by solid line and activated sensors by red (shaded) color.

The above algorithm presented in Points 1 and 3 were validated in the context of the laboratory tests presented in the next section and the data analysis performed on real structures (see Figure 13 left).

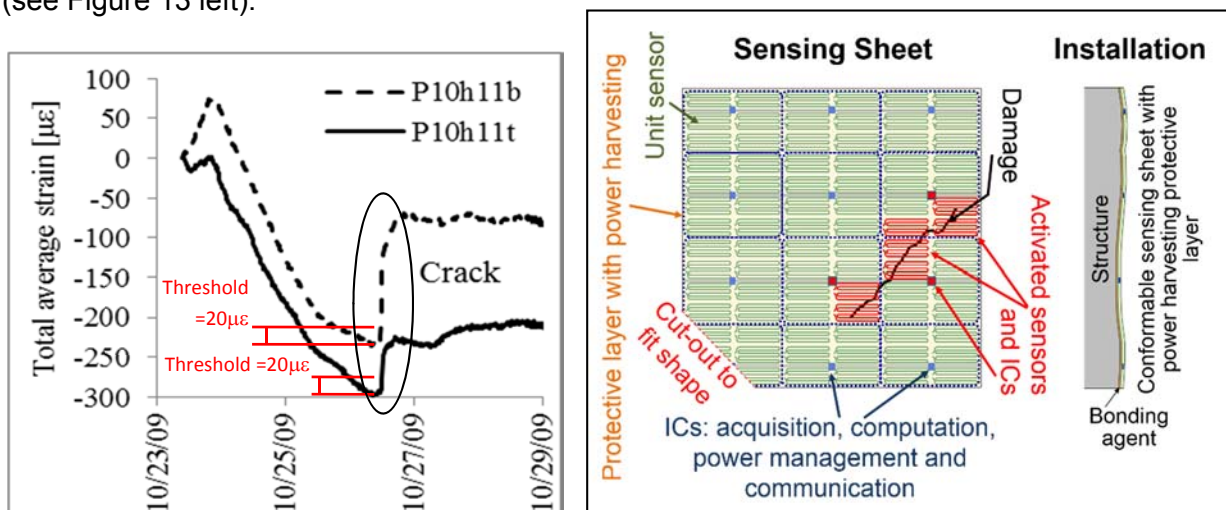


Figure 13. Left: crack detection on a real concrete structure using long-gauge fiber optic sensors and threshold-based algorithm; Right: schematic representation of the 2D LAE sensing sheet, its application, and determination of damage extent.

Implementation of traditional acoustic emission source location algorithm

Source localization was performed automatically using an algorithm based on an iterative method proposed by Geiger in 1910. This method was first developed in seismology for locating epicenters of earthquakes using only the arrival times at different geostations. It represents the best known and most widely used source location method. The concept of the method states that with at least four known arrival times from an unknown AE source to four different sensors of known locations, one can locate the source of AE both in space (x, y, z) and in time (t). The arrival times of the p-wave to the elements of the piezoelectric array are fundamental for locating the source of AE. Therefore it is required to use a reliable onset picking method in order to pick those arrivals in a consistent way.

Several onset picking techniques have been proposed in literature ranging from manual to automated techniques. A wide range of pickers, for example, are based on the STA/LTA approach (Short Term Average / Long Term Average) proposed by Baer and Kratochvil (1987). Grosse et al. (2005) developed an automatic onset detection algorithm based on the Hinckley criterion and suggested it can be used for AE. Many other techniques use approaches for onset time determination based on the modeling of signals as autoregressive processes. Akaike (1974) developed an approach called Akaike Information Criterion (AIC) in which he divides a time series into locally stationary segments and models each segment as an autoregressive process. Maeda (1985) later studied the Akaike criterion and developed a formula from which the AIC function can be directly determined from the original signal. The exact onset can be then estimated easily from the determined AIC function. In this project, all the onset picking operations were performed automatically using a MATLAB coded AIC-based picker as illustrated in Figure 14. The p-wave arrivals were then extracted and used for locating the AE sources.

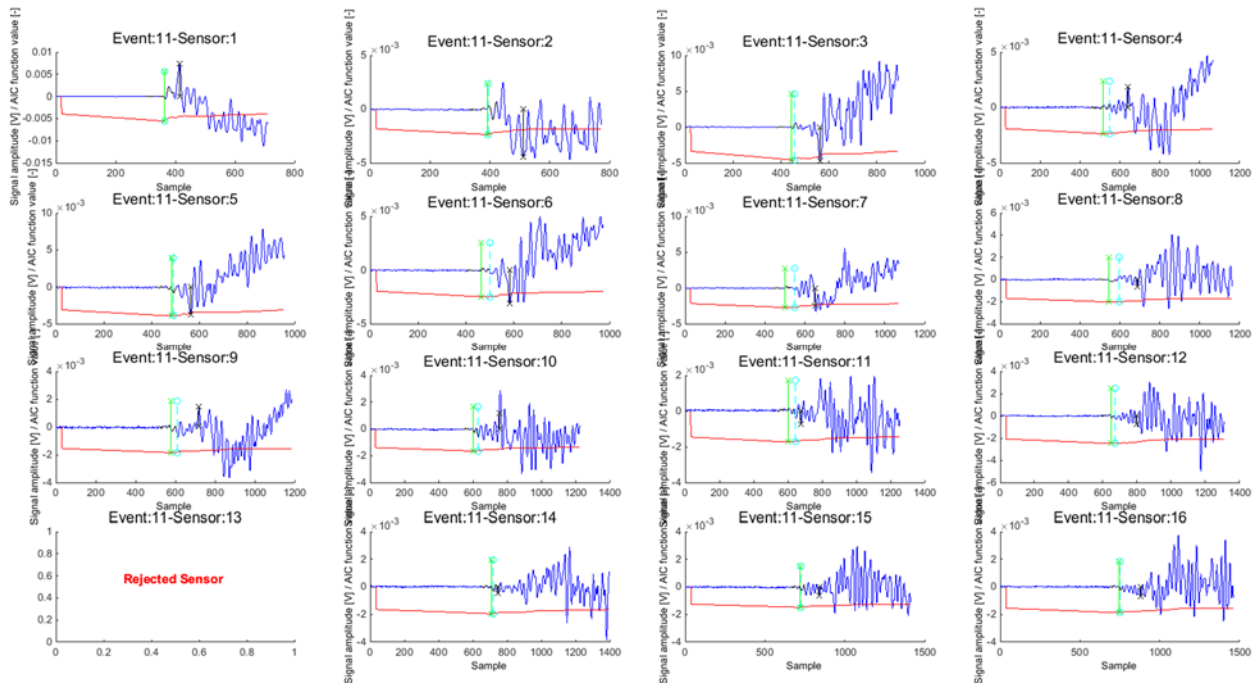


Figure 14. Sample event with 15 recorded signals and their picked arrival times using an AIC picker. The AIC function is shown in red and the picked arrival time is marked with a green vertical bar.

The AE sources in this experiment were pencil lead breaks (PLB) applied on known locations on one side of the steel plate ($y = 0.5$ in). The goal was to see whether we are able to recover the same locations if we use p-wave arrivals recorded at an array of piezoelectric discs mounted on the opposite side of the plate ($y = 0$). The first step for locating was to modify Geiger's algorithm to our problem. This was done by constraining the y -coordinate of each AE source to be $y = 0.5$ in as all the sources were all applied on one side of the steel plate. In order to do that, we forced the iterative solution inside the algorithm to have $y = 0.5$ in every single iteration so that we only estimate the remaining coordinates (x , z , and t). In general it can be said that traditional algorithms are most sensitive to uncertainties in arrival time picking and errors can become large when the source lies outside the sensor array (Schumacher 2008). More details about the derivation and implementation of the Geiger's method can be found in Ge's paper (2003).

Once the source location is estimated, the signals can be arranged with respect to their distance to the source. The slope of a linear curve fitted through the picked arrival times represents mean P-wave velocity, c_p for this result, of which an example is illustrated in Figure 15. The source time, t_0 corresponds to the point where the fitted linear curve intersects with the x -axis (at $d = 0$). The picked times are shown as a black star and one arrival time, t_{a3} , is shown for illustrative purposes.

The final result is the source coordinates (x , z , t_0) and the principal standard deviations of the estimated result can be computed and used as a measure of uncertainty.

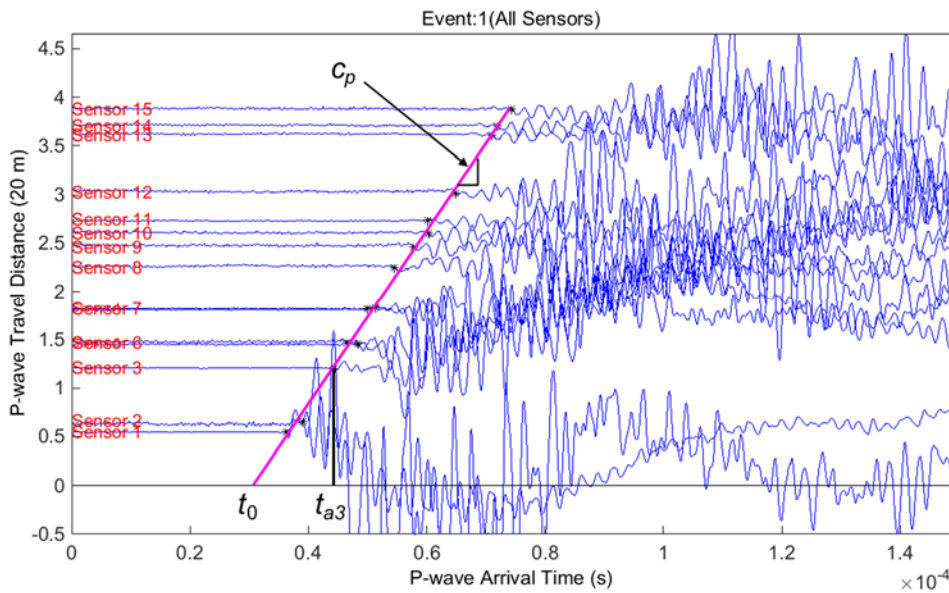


Figure 15. Example of a way to illustrate the accuracy of a located event.

Implementation of circular phased array acoustic emission source location algorithm

For circular phased arrays, the approach of phased array processing is employed of which the principle is illustrated in Figure 16.

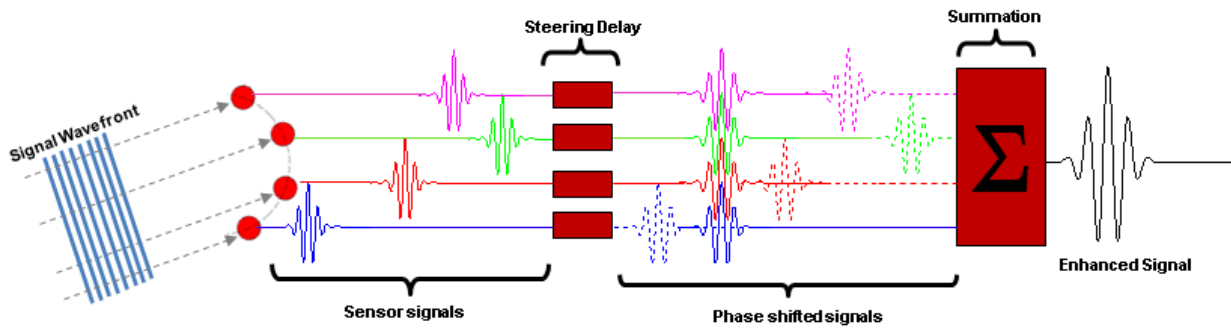


Figure 16. Schematic showing steps in phased array processing, i.e. beam forming.

The underlying assumption is that, since the source is far away, the signals collected at each sensor in a particular array are similar and only shifted in time due to the difference in distance from the source origin to each individual sensor. Another assumption that is commonly made is that of a parallel wave field, i.e. the assumption that $R = \infty$. The basic idea behind beam forming is that if the signals are summed when the correct angle for the source is assumed, and the corresponding steering delay is applied to each recorded signal, the summation of these phase shifted signals will result in a maximum response (= enhanced signal). The fundamental relationships for this algorithm are illustrated in Figure 17, where R is the distance between source and center (or radius of the wave front), and ϕ is the in-plane steering angle which is the unknown quantity to be estimated. Again, typically it is assumed that $R = \infty$.

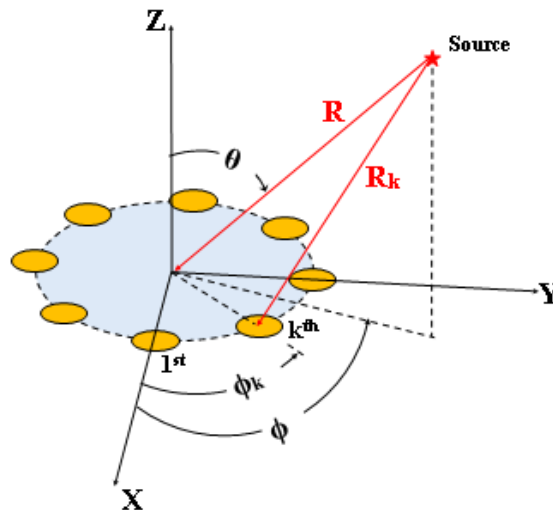


Figure 17. Parameters for beam forming using circular array.

The angle θ can be fixed to 90 Degrees to constrain the problem to two dimensions. The angle ϕ is found numerically by calculating the response for each of the stacked (= enhanced) signals for a set of finite angles. The largest response corresponds to the correct angle. If one circular array is used, the direction but not the distance, can be estimated.

This methodology was implemented in MATLAB and verified using (1) synthetically generated signals and (2) real AE signals produced from pencil lead breaks. Figure 18 shows an example of the results obtained from a circular phased array for a source located at 45 Degrees from the center of the array: (a) shows the individual AE signals recorded at each

sensor in a circular array with eight piezoelectric discs, (b) shows the total array response (maximum amplitude of stacked signals), (c) shows the power of the stacked signals for every angle from 0 to 180 Degrees in small increments (0.1 Degrees were used for this case), and (d) is a polar representation of (b) with the maximum power indicated by a red star.

The example verifies that the sensors are appropriate and the methodology to locate AE sources based on a circular phased array approach work. As can be seen in Figure 18, the actual angle of 45 Degrees was accurately predicted by the algorithm.

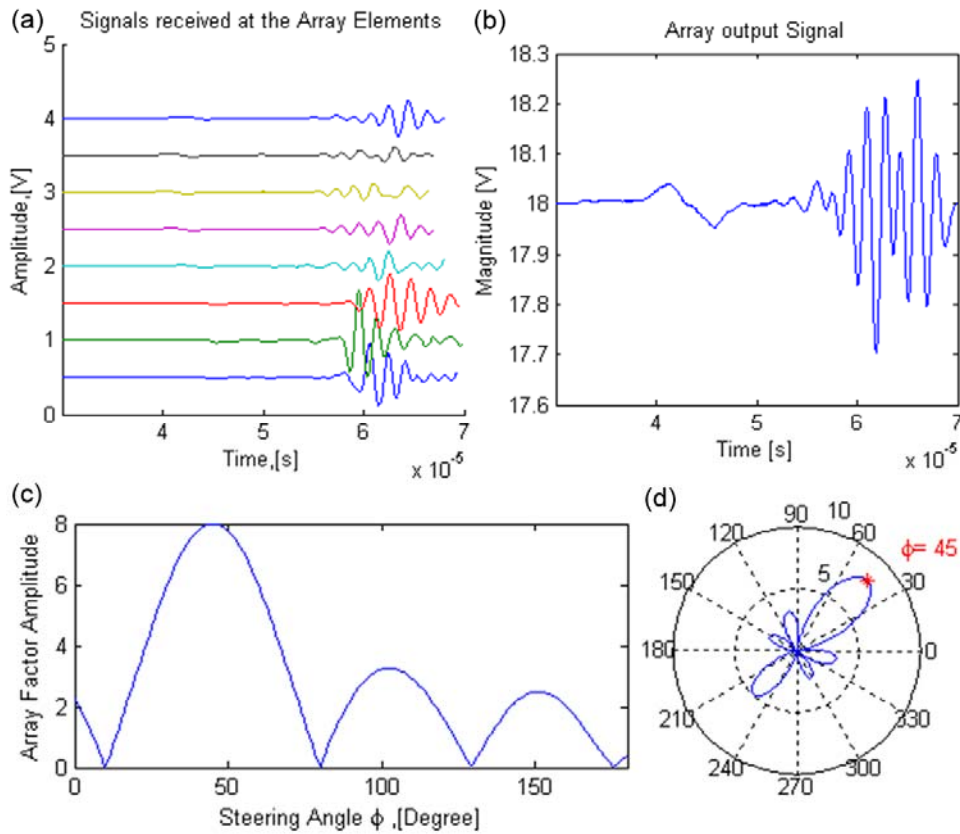


Figure 18. Example result from actual AE: (a) Individual AE signals, (b) total response for the angle corresponding to the maximum response, and results in (c) Cartesian coordinates, and (d) polar coordinates.

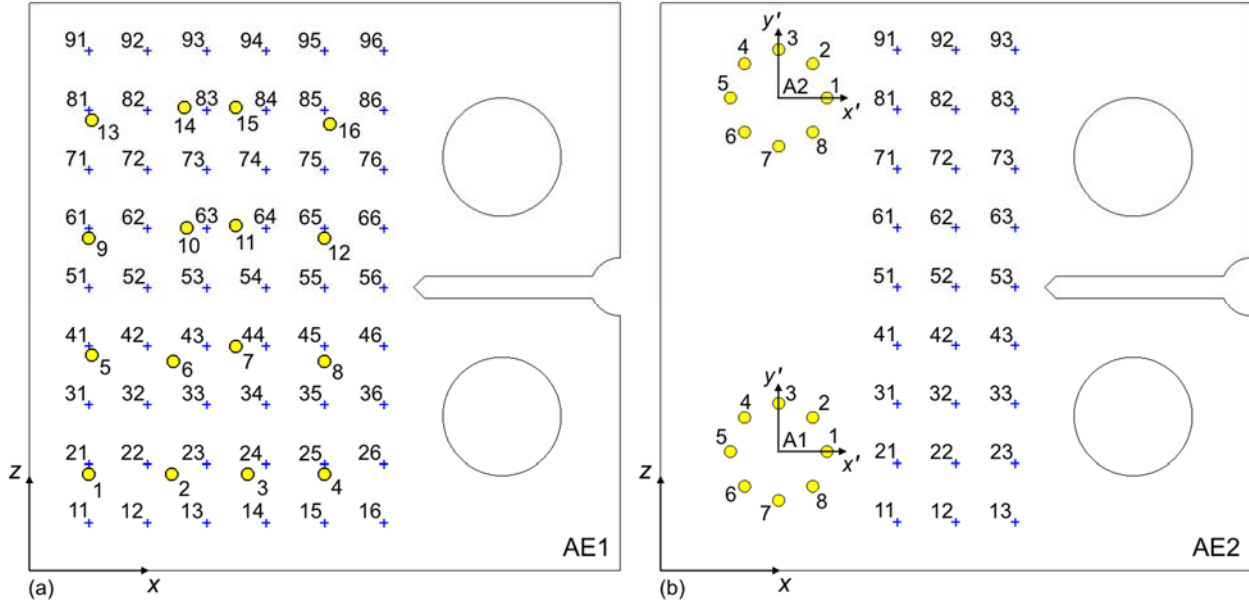
Evaluation of AE sensing sheets using artificial sources

In order to verify the proposed AE source location methodologies work, a laboratory test was performed using artificial sources applied at known locations. Since the locations were known, the predicted results could be compared with the actual location and thus the accuracy and reliability verified.

Array geometries

The two array geometries with numbering are shown in Figure 19. In order to evaluate the accuracy and reliability of the two arrays, pencil lead breaks (PLB) were performed on a 1 x 1 inch grid. For the traditional array (Figure 19 (a)) the PLBs were performed on the other face of the plate, at $y = 0.5$ in. This was done to avoid interference between the source locations (blue '+') and the piezoelectric discs (yellow circle). For the circular phased array (Figure 19 (b)) the PLBs were performed on the same face as the piezoelectric discs ($y = 0$).

Figure 19. Geometry and labeling for (a) traditional array (= AE1) and (b) circular phased array



(= AE2). Pencil lead break (PLB) locations are shown with a blue '+' and sensor locations with a yellow circle.

Traditional array

The results for the traditional array for three trials (a) to (c) are shown in Figure 20. The red stars represent the estimated source locations and the error is shown with a black line connecting the actual with the estimated source location. It can be observed that, generally, sources that are located at the border of the array are less accurately predicted compare to sources that lie within the boundaries of the array. A numerical summary is presented in Table 3.

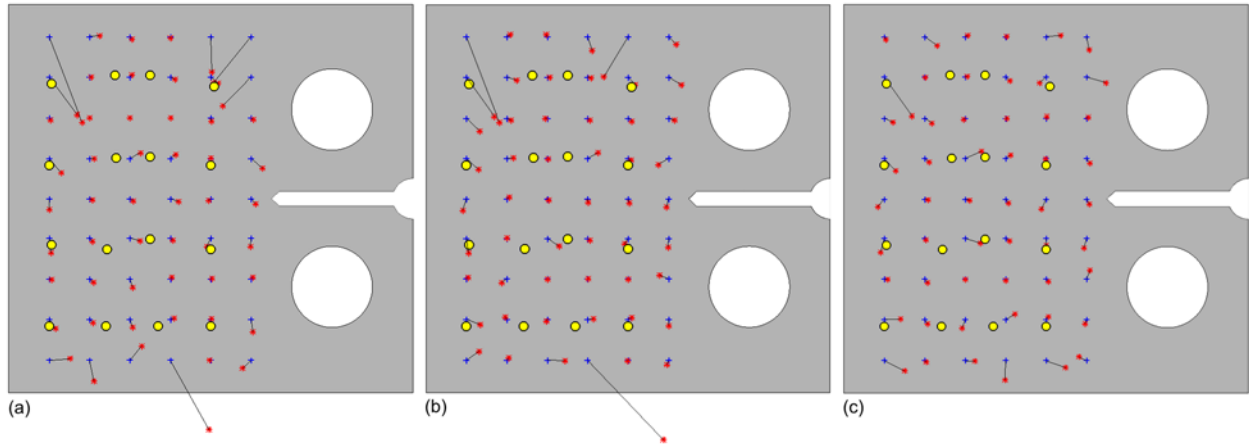


Figure 20. Located pencil lead breaks (PLB) for three trials (a) to (c) using traditional array.

Circular phased array

The results for the circular phased array for three trials (a) to (c) are shown in Figure 21. The red stars represent the estimated source locations and the error is shown with a black line connecting the actual with the estimated source location. It can be observed that the prediction errors are fairly equal and independent of the location with respect to the circular arrays. A numerical summary is presented in Table 3.

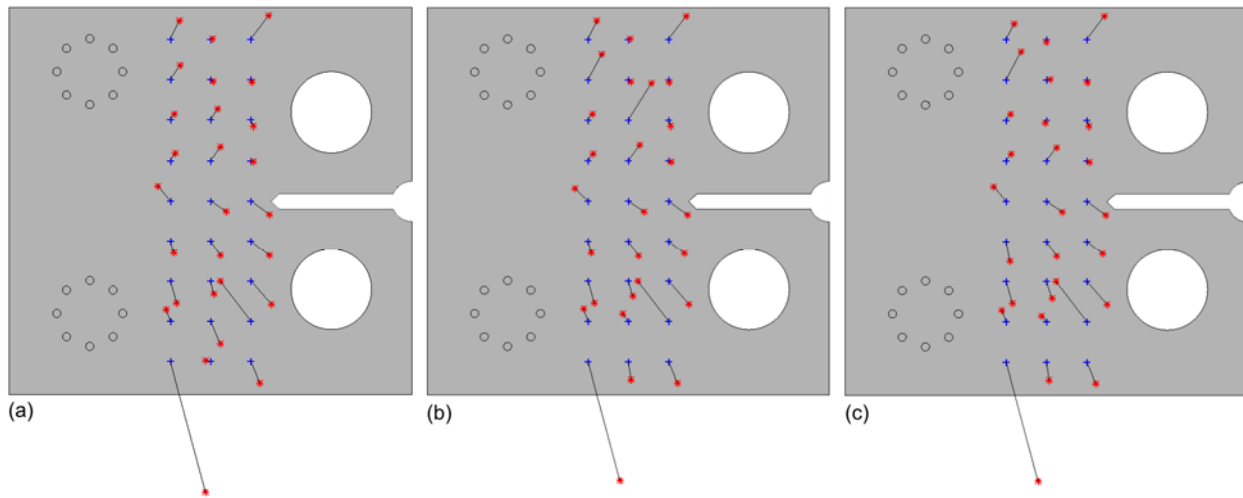


Figure 21. Located pencil lead breaks (PLB) for three trials (a) to (c) using circular phased array.

Comparison

Figure 22 and Table 3 show a comparison of errors between the source location estimates between the traditional and circular phased arrays. In order to have direct comparisons, only the locations that were used for both arrays are compared. These are locations i_4 to i_6 (for $i = 1$ to 9) and i_1 to i_3 (for $i = 1$ to 9) for the traditional and circular phased arrays, respectively. Table 3 shows the actual and estimated locations, and the computed errors in form of the distance between the two (= error vector). Figure 22 presents the average and standard deviation of the error between actual and estimated source location for all three performed trials.

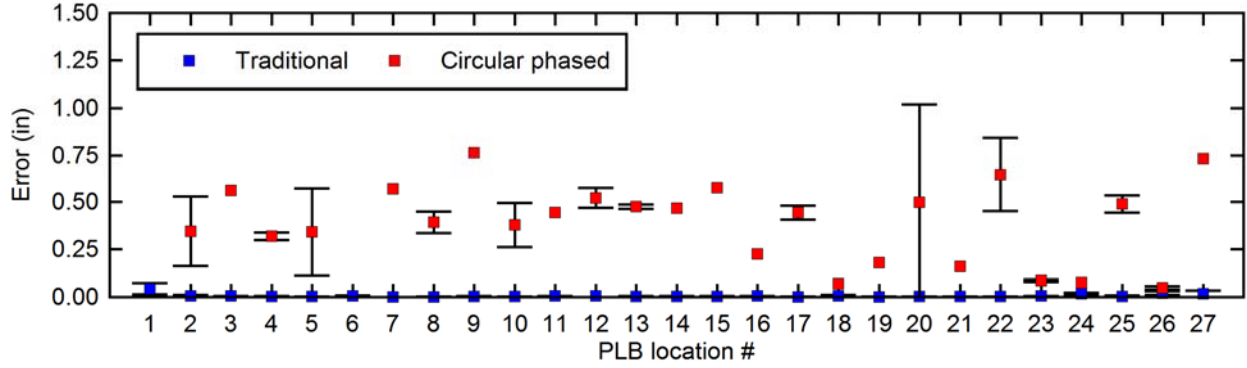


Figure 22. Comparison of source location errors for all three trials.

From this comparison, it can be concluded that the traditional algorithm is more accurate and reliable. However, the circular phased array does have advantages that should be looked at in the future. For example, they can be located in a corner of the plate, away from the damage. Also, one does not have to pick a wave mode such as the p-wave arrival, which can be an advantage in low signal-to-noise ratio environments. The idea of using two circular phased arrays has not previously been done and provides the ability to locate a source rather than just pointing in the direction of the source.

Table 3. Comparison of source location estimates with calculated errors.

#	Loc.	Traditional array					Circular phased array					
		Error			Average	StDev	Loc.	Error			Average	StDev
		Trial 1 (in)	Trial 2 (in)	Trial 3 (in)				Trial 1 (in)	Trial 2 (in)	Trial 3 (in)		
1	14	0.050	0.069	0.012	0.044	0.029	11	3.356	3.058	3.058	3.158	0.172
2	15	0.001	0.000	0.013	0.005	0.007	12	0.134	0.450	0.450	0.345	0.183
3	16	0.007	0.003	0.005	0.005	0.002	13	0.560	0.560	0.560	0.560	0.000
4	24	0.002	0.003	0.007	0.004	0.002	21	0.306	0.340	0.306	0.317	0.020
5	25	0.001	0.002	0.002	0.002	0.001	22	0.606	0.238	0.183	0.342	0.230
6	26	0.008	0.004	0.003	0.005	0.003	23	1.255	1.255	1.255	1.255	0.000
7	34	0.001	0.000	0.001	0.001	0.000	31	0.569	0.569	0.569	0.569	0.000
8	35	0.001	0.000	0.002	0.001	0.001	32	0.334	0.390	0.448	0.391	0.057
9	36	0.001	0.006	0.006	0.004	0.003	33	0.764	0.764	0.764	0.764	0.000
10	44	0.002	0.002	0.003	0.002	0.001	41	0.311	0.311	0.513	0.378	0.117
11	45	0.006	0.004	0.004	0.005	0.001	42	0.442	0.442	0.442	0.442	0.000
12	46	0.005	0.006	0.006	0.006	0.000	43	0.582	0.490	0.490	0.521	0.053
13	54	0.005	0.002	0.003	0.003	0.002	51	0.482	0.463	0.482	0.475	0.011
14	55	0.002	0.003	0.007	0.004	0.003	52	0.466	0.466	0.466	0.466	0.000
15	56	0.004	0.005	0.004	0.004	0.001	53	0.574	0.574	0.574	0.574	0.000
16	64	0.004	0.007	0.004	0.005	0.002	61	0.224	0.224	0.224	0.224	0.000
17	65	0.000	0.002	0.000	0.001	0.001	62	0.422	0.486	0.422	0.443	0.037
18	66	0.010	0.008	0.004	0.007	0.003	63	0.068	0.068	0.068	0.068	0.000
19	74	0.000	0.002	0.001	0.001	0.001	71	0.178	0.178	0.178	0.178	0.000
20	75	0.002	0.003	0.001	0.002	0.001	72	0.338	1.080	0.071	0.496	0.523
21	76	0.002	0.004	0.001	0.002	0.002	73	0.158	0.158	0.158	0.158	0.000
22	84	0.003	0.002	0.003	0.003	0.001	81	0.422	0.732	0.789	0.648	0.197
23	85	0.006	0.006	0.005	0.006	0.001	82	0.082	0.082	0.093	0.085	0.006
24	86	0.025	0.010	0.013	0.016	0.008	83	0.075	0.075	0.075	0.075	0.000
25	94	0.001	0.009	0.001	0.004	0.005	91	0.515	0.515	0.436	0.489	0.046
26	95	0.022	0.029	0.009	0.020	0.010	92	0.043	0.043	0.059	0.048	0.009
27	96	0.037	0.007	0.008	0.018	0.017	93	0.732	0.732	0.732	0.732	0.000

Laboratory experiments

Test description

The large-scale tests on steel plates equipped with sensing sheets were carried out at the Carleton Laboratory in Columbia University. Measurement devices for the fatigue tests were brought onsite by each research partner. To reduce the costs, conventional reading units were used: (1) National Instruments with 32 channels switching capability (NI 9219 4 Ch-Ch Isolated, 24-bit, Universal AI Module with cDAQ-9178, CompactDAQ chassis) for strain sensors and (2) Elsys TraNET transient recorder with high-speed 16 channels (can sample up to 40 MHz at 14 bit depth).

The fatigue test device with specimen fixtures are shown in Figure 23. The MTS machine was used to apply cyclic fatigue load, and the pair of fixture to hold the test samples was installed in the middle. The test samples were further protected for insulation with duct tape. Then they were hooked up to the fixture and secured using two steel pins (see Figure 23).



Figure 23. Left: fatigue test setup and test fixture; Middle: installation of specimen; Right: specimen insulated with duct tape, placed into the testing frame, secured with the fixtures, and connected with cables (to the reading unit).

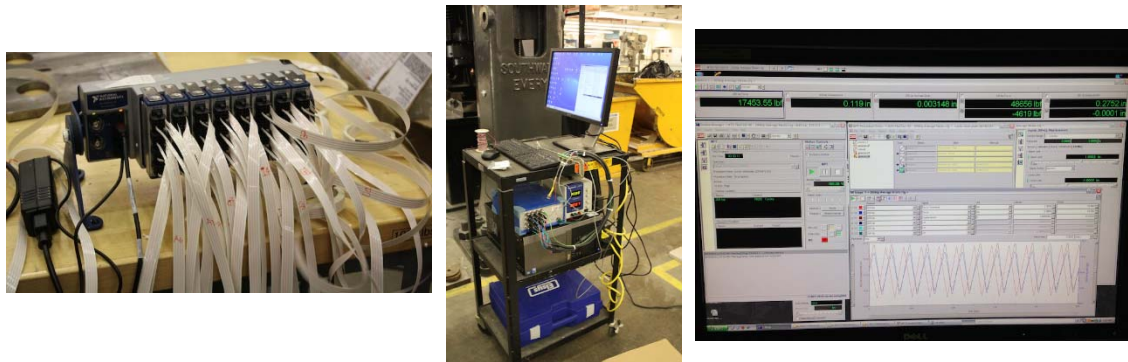


Figure 24. Left: Strain signal reading unit of Princeton University; Middle: Acoustic emission signal reading unit of University of Delaware; Right: MTS displacement and load control system of Columbia University.

The sensing sheets were connected to each reading unit with cables (see Figure 23). Princeton research group recorded strain, the University of Delaware research group recorded acoustic emissions caused by fracture events, and Columbia research group registered fatigue displacement and load value. All the readings were performed in real-time. Photos of the reading units used by three universities is shown in Figure 24.

The specimens (see Table 1, and Figures 6 and 7) were tested in the following order:

Specimen No. 2:

No. of loading cycles: 0-110,000;
Actual load range: 12kip-20kip;
Loading frequency: 4 Hz (4 cycles per second);
Sampling rate for strain sensors: 20 Hz;
Sampling rate for AE sensors: 5 MHz at 16 bit using voltage threshold crossing
No. of loading cycles: 110,001-139,913 (specimen failed at this stage);
Actual load range: 13kip-24kip;
Loading frequency: 6 Hz (6 cycles per second)
Sampling rate for strain sensors: 20 Hz;
Sampling rate for AE sensors: 5 MHz at 16 bit using voltage threshold crossing.

Specimen No. 4:

No. of loading cycles: 0-58,867 (test sample failed at this stage);
Actual load range: 12kip-25kip (initial), 14kip-23kip (final);
Loading frequency: 6 Hz (6 cycles per second);
Sampling rate for strain sensors: 20 Hz.
Sampling rate for AE sensors: 5 MHz at 16 bit using voltage threshold crossing.

Specimen No. 3:

No. of loading cycles: 0-135,645 (test sample failed at this stage);
Actual load range: 20kip-28kip;
Loading frequency: 4 Hz (4 cycles per second);
Sampling rate for strain sensors: 20 Hz.
Sampling rate for AE sensors: 5 MHz at 16 bit using voltage threshold crossing.

Specimen No. 1:

No. of loading cycles: 0-99,696 (test sample failed at this stage);
Actual load range: 20kip-28kip;
Loading frequency: 4 Hz (4 cycles per second);
Sampling rate for strain sensors: 20 Hz.
Sampling rate for AE sensors: 5 MHz at 16 bit using voltage threshold crossing.

During the cycling tests the tip of the notch zone in the steel plate would suffer the largest stress concentration, and the initial fatigue crack was expected to occur at that location. Based on the four test observations, the initial crack appeared before 40,000 cycles are carried out. Figure 22 shows the initial cracks in Specimens No. 1 and 2. Under the cycling that followed the initiation, the crack propagation was very slow and it started to propagate faster only when the specimen was close to failure. The specimen was considered as failed when the vertical distance between the two fixture pins had reached one inch, and at that stage the crack ended in the area close to the middle of the plate.

During the failure process, the shaking of the specimens caused the interconnect sheets to delaminate; however, individual sensors were still bonded well on the steel plate. Figure 23 shows the examples of the failure of the sensing sheets under extreme crack opening. Two main mechanisms of the sheet failure were noticed: delamination and tearing. It is important to note that as the initial crack crossed the first closest sensor, this sensor would be damaged immediately. However, the other sensors would continue functioning until either they are damaged or the interconnect is damaged by one of the above presented failure modes.

Immediate damaging of the strain sensor is different from the findings made on concrete specimens (see Figures 1 and 2), where the sensor functioned properly until few millimeter crack was formed. The main reasons for this difference are (1) better adhesion of the sheet to the steel than to the concrete and (2) degradation of concrete in the zone of the crack opening that does not occur in the case of steel. Hence, the response of the unit strain sensor exposed to crack is different for steel and concrete, and the use of softer adhesive is advised for the installation of the sensing sheet to the steel elements.

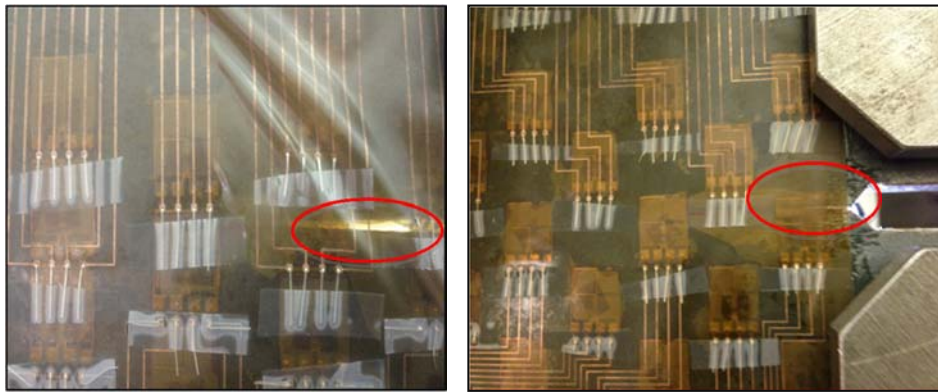


Figure 25. Initial crack occurring in Specimen No. 1 (left) and No. 2 (right).

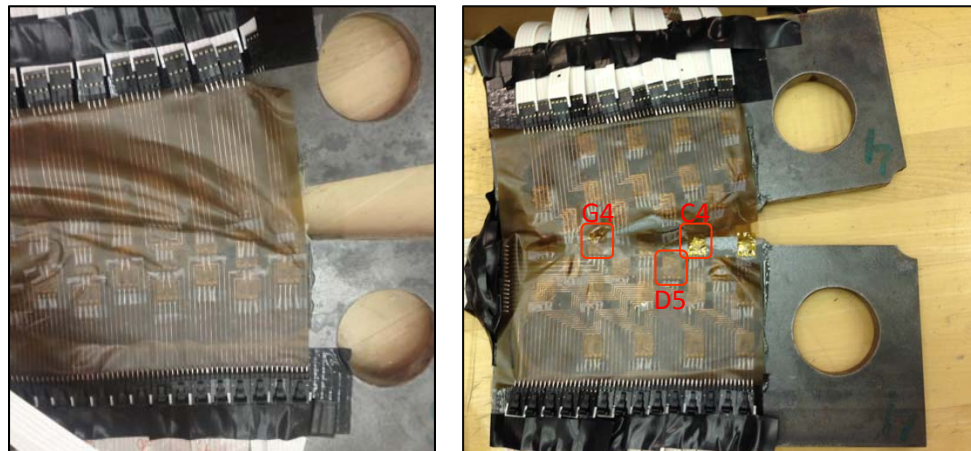


Figure 26. Typical failure modes of the sensing sheet under excessive crack opening; Left: delamination, Sample No.; 3; Right: tearing, Specimen No. 4.

Measurement results from strain sensing sheets

To illustrate the general response of strain sensors from the sensing sheets, three typical individual sensors from Specimen No. 4 are presented.

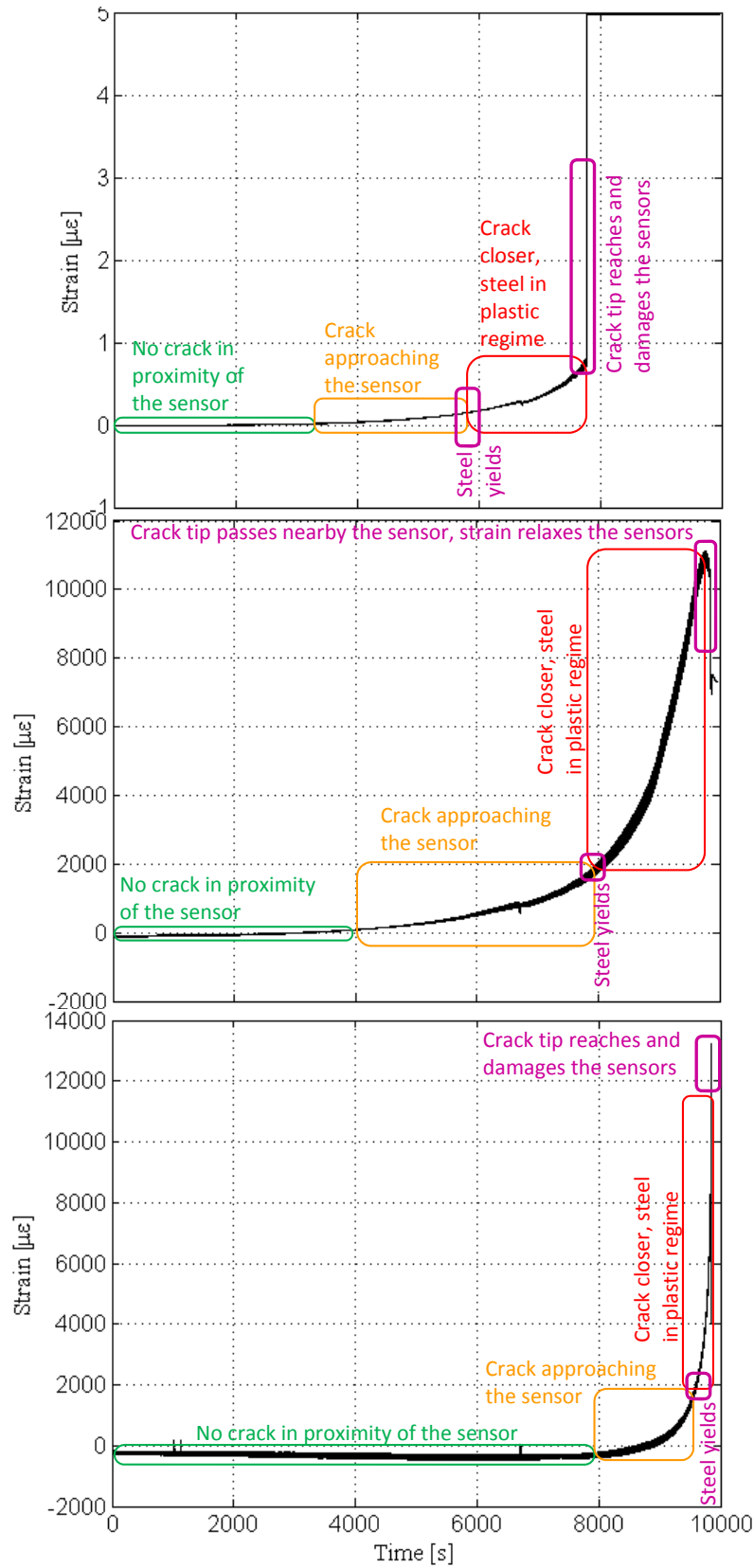


Figure 27. Typical sensor readings, Specimen No. 4.

The selected examples are sensors with coordinates *C4*, *D5* and *G4* and these sensors are encircled in Figure 26. Note that crack propagates from side *A* towards *I* (see Figure 6) i.e., it first meets sensor with coordinate *C* and then propagates towards the sensors with coordinates *D* and/or *G*. Figure 26 shows that the sensor *C4*, which was on the crack, was clearly broken by it; sensor *D5* is not at the location of the crack, but below it, and thus it was not damaged by crack; finally, sensor *G4* was on the crack propagation line, and the crack tip reached it, so this sensor was damaged.

The time series of the three sensors are shown in Figure 27. Important events are shown in each diagram. Detailed presentation on crack “passing” nearby position *D* and reaching position *G* is shown in Figure 28.

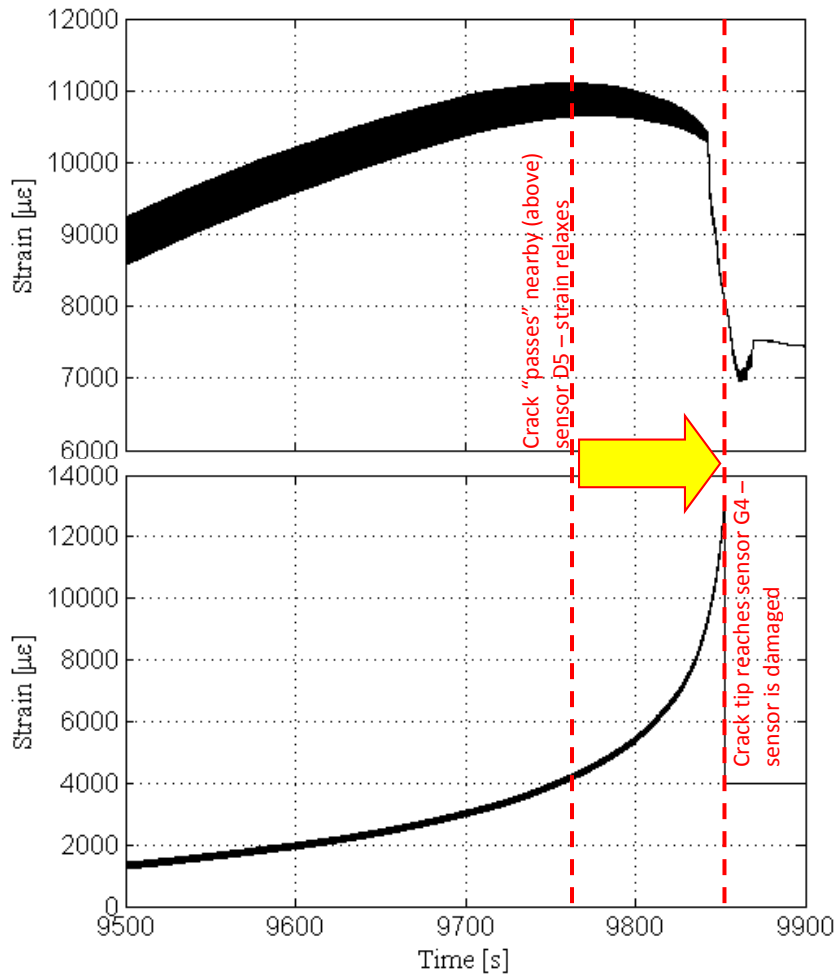


Figure 28. Propagation of crack from location “D” to location “G”.

The tests have demonstrated that the sensing sheet could perform reliable crack detection and could follow crack propagation in-time. This is important finding as it proves the concept of direct sensing applied to dense arrays of strain sensors, and validates the idea of the sensing sheet. In addition, the tests helped identify several directions for future research.

The sensors that were in contact with the crack would be immediately damaged, indicating that either softer adhesive should be used or the sensor should be made of more ductile material (or both).

While Design 2 had benefits of denser sensor array, the Design 1 was also successful in damage detection and evaluation, indirectly, through relaxation of sensors. This is very important as it shows that even less dense networks could be successful in damage characterization, which may significantly simplify manufacturing of sensing sheets and data analysis.

Measurement results from AE sensing sheets

Figures 29 and 30 show examples of acoustic emissions recorded at all channels during the fatigue test. Unfortunately, it turns out that these signals did not look like real AEs. There are several plausible reasons that will have to be investigated. The event capture in Figure 29 is likely due to small surges in the electric system. Figure 30 shows a noisy signal with some low-frequency signal content. Unfortunately, these signals are difficult to filter and our transient recorder does not allow for elaborate preprocessing and visualization of the captured signals. Since we don't believe these signals are real, i.e. caused by fatigue cracking, we cannot do any further analysis at this point. The lessons learned are that extensive preliminary testing in the environment and with realistic background noise needs to be conducted in the future prior to actual testing. Isolation of background noise and electrical surges is essential to avoid any false triggering observed here.

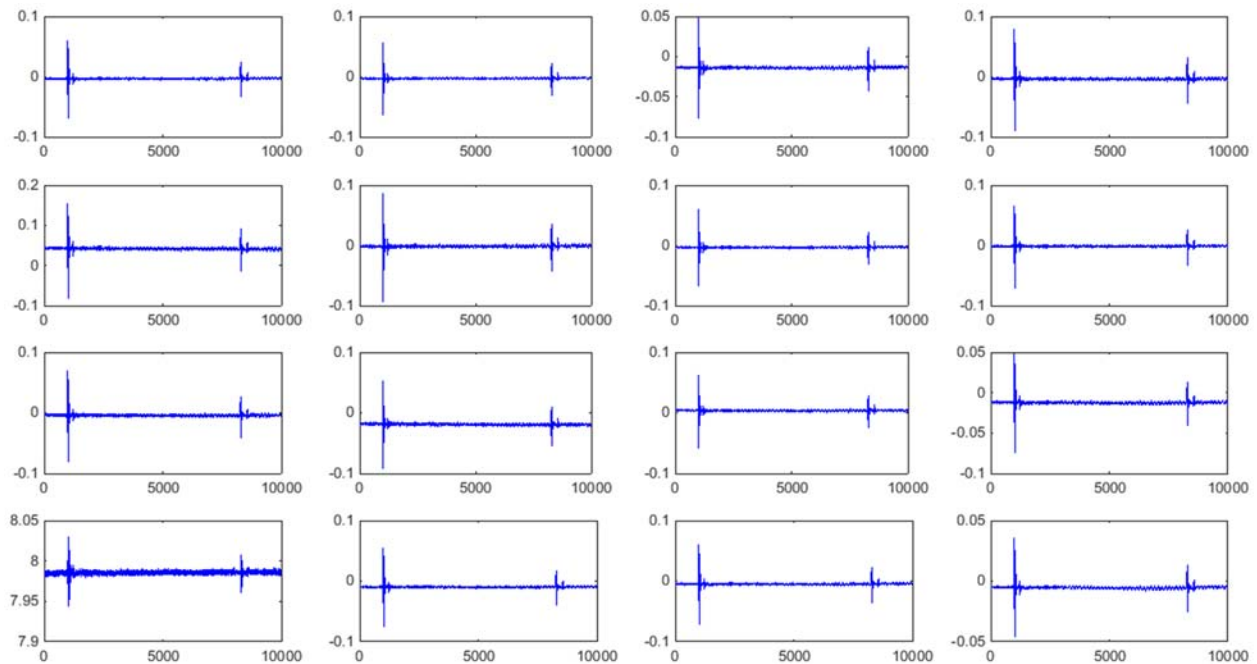


Figure 29. Example of AE signal due to short electric surges.

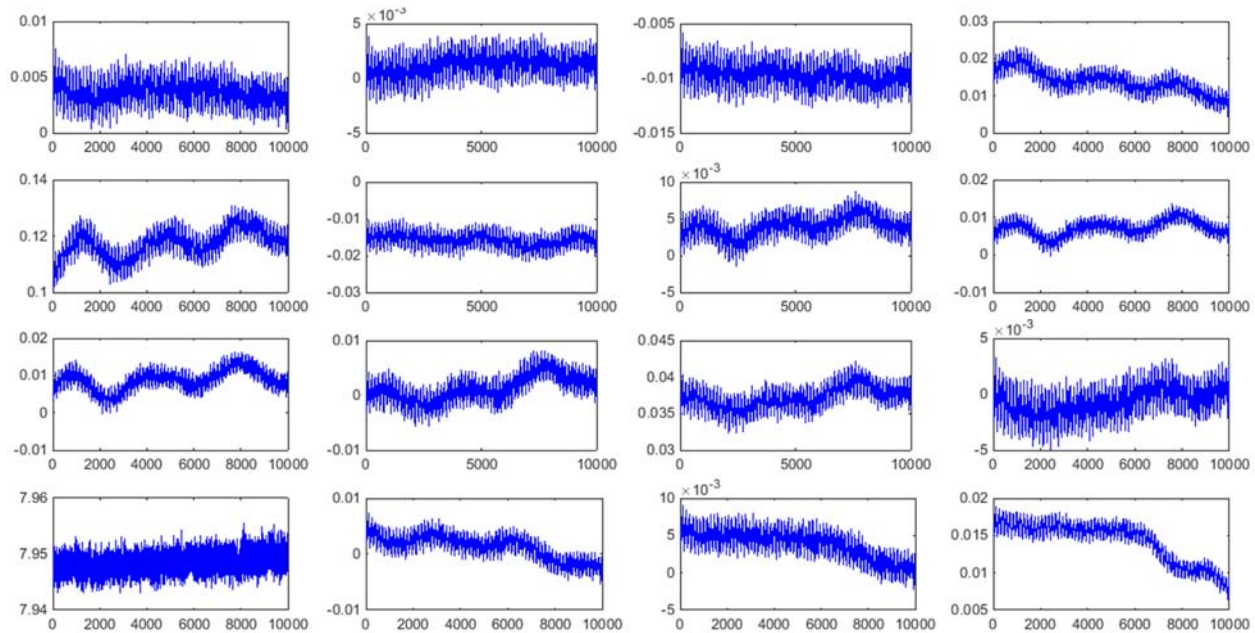


Figure 30. Example of AE signal due to low-frequency noise.

CONCLUSIONS

Several major conclusions can be drawn from this project:

1. The literature review revealed a need for two dimensional dense arrays of sensors for detection and characterization of local damage such as crack. This finding justified research on sensing sheet.
2. The sensing sheet with multi-sensing properties, i.e., based on strain sensors and acoustic emission (AE) sensors has been researched. The unit sensing elements for sensing sheet, i.e., the resistive strain sensor in bridge configuration and AE piezo-electric discs were identified and characterized in laboratory conditions.
3. The bridge configuration was chosen for strain sensor as its differential sensing characteristics minimize the noise from environment. It was demonstrated in reduced-scale tests that the sensor can estimate the size of crack opening occurring on concrete using probabilistic approach. However, the crack size cannot be estimated on steel elements and further research is needed to achieve this aim (see the next section).
4. Two different AE sensor arrays were implemented and tested to locate AE in finite-size plate-like steel plates: traditional array using source location algorithm based on arrival time differences and circular phased array using beam forming.
5. The design of strain sensing sheet was determined based on the concept of probability

of detection. The theoretical derivations resulting from this analysis can be used in broader sense for any strain network in a structure. Two designs were identified as potentially successful and tested in large-scale tests. Both designs performed well in the tests, but also generated new findings that indicate directions of future research.

6. Two separate AE source location algorithms were implemented in MATLAB. The novelty of the circular phase array approach is that we use two separate arrays, which allows for estimating the actual location rather than just the direction of the source. This has not been done previously.
7. The algorithms for damage detection were created and successfully applied in data analysis for strain sensing sheet. The algorithms are based on thresholds defined based on modified Z-score applied to moving windows of measurements and yield strain limits.
8. Both AE sensor arrays were designed using piezoelectric discs and evaluated by performing pencil lead breaks at known locations. Since the locations were known, the absolute estimation error could be computed. Overall, the traditional array using arrival time differences was more accurate and reliable. Although the circular phased array had larger estimation errors, it has the advantage that the sensors are far away from the damage and no wave mode has to be picked. Although the AE sensing sheets performed well for the pencil lead breaks, they were not able to detect the relatively low amplitude events caused by steel fatigue cracking. This may have to do with the noisy testing environment.
9. The sensing sheet prototypes were manufactured by laminating the commercially available sensors over patterned interconnect, and tested in large-scale tests on a steel specimens subjected to cycling loading and fatigue cracking.
10. In overall the results of the project are satisfactory. The concept of sensing sheet was proven in large-scale tests, and its reliability in crack detection and capability of tracking the crack propagation validated. Several publications resulted from the project (see below), and recommendations for future research are identified and presented in the next section.

Publications resulting from the project:

Journal Papers

1. Tung, S-T, Glisic, B. (2015). Sensing Sheet: The Response of Full-Bridge Unit Sensors to Thermal Variations for Crack Detection and Characterization, Measurement Science and Technology (in preparation).
2. Yao, Y., Glisic, B. (2015). Detection of steel fatigue cracks with strain sensing sheets based on large area electronics, Sensors, 15: 8088-8108.
3. Tung, S-T., Yao, Y., Glisic, B. (2014). Sensing Sheet: The Sensitivity of Thin-Film Full-

Bridge Strain Sensors for Crack Detection and Characterization, Measurement Science and Technology, 25(7), art. no. 075602 (14pp).

4. Yao, Y., Tung, S-T. E., Glisic, B. (2014). Crack detection and characterization techniques – an overview, Structural Control and Health Monitoring, 21(12): 1387–1413.

Conference papers:

1. Yao, Y., Glisic, B. (2014). Probabilistic Damage Detection Based on Large Area Electronics Sensing Sheets, 7th European Workshop on Structural Health Monitoring (EWSHM), Nantes, France, July 8-11, 2014, paper on conference CD.
2. Yao, Y., Tung, S-T., Glisic, B. (2014) High-resolution sensing sheet for damage detection based on large area electronics, The 7th International Conference on Bridge Maintenance, Safety and Management (IABMAS), Shanghai, China, July 7-11, 2014, paper on conference CD.
3. Tung, S-T.E., Yao, Y., Glisic, B. (2014). Crack identification based on thin-film full-bridge strain sensors, Proceedings of SPIE - The International Society for Optical Engineering 9061 - 33.
4. Yao, Y., Tung, S-T.E., Verma, N., Glisic, B. (2013). High-resolution sensing sheet for damage detection based on large area electronics, 6th International Conference on Structural Health Monitoring of Intelligent Infrastructure (SHMII-6), Hong Kong, China, paper on conference CD.
5. Glisic, B., Yao, Y., Sigurdardottir, D. (2013). Two probabilistic damage detection approaches, 6th International Conference on Structural Health Monitoring of Intelligent Infrastructure (SHMII-6), Hong Kong, China, paper on conference CD.
6. Yao, Y., Tung, S-T.E., Verma, N., Glisic, B. (2013). Towards sensing sheets based on large area electronics, The 9th International Workshop on Structural Health Monitoring, Stanford University, paper on conference CD.

RECOMMENDATIONS

The tests have demonstrated that the sensing sheet could perform reliable crack detection and could follow crack propagation in-time. The following recommendations are proposed based on experience and test results from the project:

1. Selection of the unit strain sensor: resistive strain sensor in bridge configuration was proven to be robust to external influences; thus, this type of sensor is recommended for the future research and development of the strain sensing sheet.
2. Manufacturing of the strain sensing sheet: while laminating the strain sensors over the sensing sheet interconnect, it is highly recommended to weld the sensor leads to corresponding interconnect pads; simple physical contact ensured by ordinary adhesive tape is not sufficient to maintain reliable contact in even short-terms.

3. Installation of the strain sensing sheet onto the steel elements: while gluing the sensing sheet to steel elements it is recommended to use soft adhesive (research of an appropriate adhesive is necessary); soft adhesive may prevent premature rupture of the sensor exposed to crack. Alternatively, new sensor made of more ductile material (e.g., conductive polymer) could be researched and used.

In the case of installation on concrete elements, the tested adhesive (Araldite 2012) can be used as the degradation of concrete around the crack will reduce the transfer of concentrated stresses to the sensor and in turn help the sensor to “survive” the crack opening.

4. Design of the strain sensing sheet: the sensors that are close to cracks, but not in direct contact with it are shown to be able to detect the crack by strain relaxation; this is very important as it demonstrates that even less dense networks could be successful in damage characterization, which may significantly simplify manufacturing of sensing sheets and data analysis. Consequently, it is recommended to expand the developed method for evaluation of probability of detection (POD), which based on contact with damage, to accommodate for evaluation of POD for sensors that are not in direct contact with damage. This research will involve detailed analysis of strain field changes in proximity of the damage (i.e., in proximity of crack).
5. The AE sensing methodology should be further evaluated. In particular, the proposed circular phased array approach, although giving results, needs to be improved. Also, the AE sensing sheets need to be retested on real sources before large-scale testing is performed. Some of the additional tests that could be done include analog filtering of signals to avoid triggering of the transient recorder by low-frequency noise and better noise-control of experimental setup.
6. Once the above recommendations are implemented, further large-scale testing of the sensing sheet is needed; successful outcomes will eventually lead to deployment and testing of the sensing sheet in real-life settings.